A genome-wide analysis of adhesion in *Caulobacter crescentus* identifies new regulatory and biosynthetic components for holdfast assembly

David M. Hershey[1], Aretha Fiebig[1] and Sean Crosson[1,2]*

[1] Department of Biochemistry and Molecular Biology, University of Chicago, Chicago, IL 60637, USA.

[2] Department of Microbiology, University of Chicago, Chicago, IL 60637, USA.

* To whom correspondence should be addressed: scrosson@uchicago.edu; (773) 834-1926

Running title: Genome-wide analysis of adhesion

Keywords: holdfast, adhesion, polysaccharide, *Caulobacter*, BarSeq, pilus

Abstract: Due to their intimate physical interactions with the environment, surface polysaccharides are critical determinants of fitness for bacteria. *Caulobacter crescentus* produces a specialized structure at one of its cell poles called the holdfast that enables attachment to surfaces. Previous studies have shown that the holdfast is a carbohydrate-based material and identified a number of genes required for holdfast development. However, incomplete information about its chemical structure, biosynthetic genes and regulatory principles has limited progress in understanding the mechanism of holdfast synthesis. We have leveraged the adhesive properties of the holdfast to perform a saturating screen for genes affecting attachment to cheesecloth over a multi-day time course. Using covariance in the temporal profiles of mutants in a transposon library, we defined discrete clusters of genes with related effects on cheesecloth colonization. Holdfast synthesis, flagellar motility, type IV pilus assembly and smooth lipopolysaccharide (SLPS) production represented key classes of adhesion determinants. Examining these clusters in detail allowed us to predict and experimentally define the functions of multiple uncharacterized genes in both the holdfast and SLPS pathways. In addition, we showed that the pilus and flagellum control holdfast synthesis separately by modulating the holdfast inhibitor *hfiA.* This study defines a set of genes contributing to adhesion that includes newly discovered genes required for holdfast biosynthesis and attachment. Our data provide evidence that the holdfast contains a complex polysaccharide with at least four monosaccharides in the repeating unit and underscore the central role of cell polarity in mediating attachment of *C. crescentus* to surfaces.

Importance: Bacteria routinely encounter biotic and abiotic materials in their surrounding environments, and they often enlist specific behavioral programs to colonize these materials. Adhesion is an early step in colonizing a surface. *Caulobacter crescentus* produces a structure called the holdfast, which allows this organism to attach to and colonize surfaces. To understand

39 how the holdfast is produced, we performed a genome-wide search for genes that contribute to
40 adhesion by selecting for mutants that could not attach to cheesecloth. We discovered complex
41 interactions between genes that mediate surface contact and genes that contribute to holdfast
42 development. Our genetic selection identified what likely represents a comprehensive set of genes
43 required to generate a holdfast, laying the groundwork for a detailed characterization of the
44 enzymes that build this specialized adhesin.
45
46 **Introduction:** The bacterial cell envelope is a highly dynamic structure that is essential for growth
47 and division(1). Carbohydrate-based compounds often form the outermost layer of the envelope,
48 comprising a specialized surface that each cell displays to the surrounding environment(2). The
49 roles of surface polysaccharides such as capsules, exopolysaccharides and O-antigens in
50 promoting colonization of preferred niches are well established for both free-living and infectious
51 bacteria(3-5). However, the enzymes that synthesize and export these polysaccharides have been
52 difficult to characterize due to the chemical complexity of the metabolic intermediates(6).
53 Defining the molecular details of how extracellular carbohydrates are produced is critical to
54 understanding bacterial colonization and how it can be controlled.
55 The aquatic bacterium *Caulobacter crescentus* has a dimorphic lifestyle characterized by an
56 association with exogenous surfaces. Division in *C. crescentus* is asymmetric and produces two
57 distinct cell types, a chemotactic swarmer cell and a sessile, replication-competent stalked cell(7).
58 After replication initiation, a swarmer cell sheds its flagellum, disassembles its pili and undergoes
59 a transition into a stalked cell before dividing(8). Stalked cells are named for a specialized
60 envelope extension called the stalk that emerges from the new pole after disassembly of the
61 flagellum and pili. During the swarmer to stalked transition, cells often produce a polysaccharide

62 rich matrix called the holdfast at the site of stalk development(9). This highly adhesive material
63 allows *C. crescentus* to form essentially permanent interactions with exogenous surfaces (Fig 1A).
64 Due to the irreversible nature of surface attachment in *C. crescentus*, the timing of holdfast
65 production is tightly controlled. When grown in defined medium only a small proportion of cells
66 produces a holdfast, as compared to nearly all cells when grown in complex medium(10). This
67 effect is due to elevated expression of the *holdfast inhibitor A* (*hfiA*) gene in defined medium (Fig
68 1B). *hfiA* expression is also coordinated with the cell-cycle. Its transcript levels drop during the
69 swarmer to stalked transition, which corresponds to the developmental stage at which holdfasts
70 begin to appear. Numerous signaling pathways target the *hfiA* promoter, allowing the cell to
71 integrate environmental, nutritional and developmental cues into a single output that regulates
72 adhesion(10, 11). In yet another regulatory regime, holdfast synthesis can be induced when a
73 swarmer cell encounters a surface(12). Physical disruption of flagellar rotation or pilus oscillation
74 upon surface contact stimulates the production of a holdfast (13, 14). How the numerous
75 regulatory pathways converge to control holdfast development remains unclear, but the
76 complexity of these networks reflects the significance of committing to a surface-associated
77 lifestyle.
78 Genetic analysis of non-adhesive mutants indicates that the holdfast is a polysaccharide-
79 based material. The holdfast synthesis (*hfs*) genes include predicted glycosyltransferases,
80 carbohydrate modification factors and components of a *wzy*-type polysaccharide assembly
81 pathway(15-18). *wzy*-dependent carbohydrate assembly utilizes a lipid carrier known as
82 undecaprenylpyrophosphate (UPP) on which glycosyltransferases assemble an oligosaccharide
83 repeating unit(19). The resulting glycolipid is flipped from the cytoplasmic face of the inner
84 membrane to the periplasmic face where the oligosaccharide is polymerized and exported to the
85 cell surface(20). The *wzy* mechanism is used to produce an impressive diversity of

86 polysaccharides and is broadly conserved among bacteria(21). Thus, characterizing enzymes
87 involved in the biosynthesis of the holdfast has the potential to uncover broadly applicable
88 principles about how bacteria produce carbohydrate polymers.

89 The chemical nature of the holdfast matrix remains poorly characterized. The holdfast
90 binds to the N-acetylglucsoamine (GlcNAc) specific lectin wheat germ agglutinin (WGA) and is
91 sensitive to the GlcNAc specific hydrolases cellulase and lysozyme, indicating that GlcNAc is a
92 component of the matrix(22). Little other information about the carbohydrate content has been
93 reported. Extracellular DNA and unidentified protein component(s) also contribute to the
94 mechanical properties of the holdfast, but only mutations in polysaccharide biosynthesis genes or
95 pleiotropic regulators of cell polarity abolish holdfast production(23). Currently, three
96 glycosyltransferase steps are known to be required for holdfast synthesis. An initial reaction
97 carried out by one of the genetically redundant HfsE, PssY or PssZ enzymes is thought to be
98 followed by the actions of HfsG and HfsJ, suggesting that the polysaccharide may be composed of a
99 triscaccharide repeat(10, 17). However, new *hfs* genes continue to be discovered, hinting that
100 additional glycosyltranferases may remain unidentified(10, 24). Uncertainty about both the
101 composition of the holdfast and the saturation of screens for *hfs* genes presents a major obstacle
102 to characterizing enzymatic reactions in the pathway.

103 Here, we utilized saturating transposon mutagenesis to probe holdfast production at the
104 genome scale. We developed a barcoded transposon library in *C. crescentus* and enriched for non-
105 adhesive mutants by passaging across multiple days in presence of cheesecloth. We discovered a
106 surprising number of genes with distinct adhesion phenotypes that ranged from hyper-adhesive
107 to non-adhesive. We found that disrupting the smooth lipopolysaccharide (SLPS) leads to ectopic
108 adhesion throughout the cell surface, and we used the temporal adhesion profile of known SLPS
109 mutants to identify and characterize new genes in the SLPS pathway. The same covariance

110 approach was used to place previously uncharacterized genes in the holdfast pathway. We further
111 demonstrated that disrupting the assembly of polar surface appendages modulates the activity of
112 the holdfast inhibitor, *hfiA.* In particular, individual mutations in the pilus machinery had a range
113 of adhesion phenotypes suggesting that distinct intermediates in the pilus assembly pathway have
114 opposing effects on *hfiA*. Based on our comprehensive analysis of holdfast regulation, biosynthesis
115 and assembly, we propose a model that outlines the complete set of enzymatic steps required to
116 produce the holdfast polysaccharide.
117
118 **Results:**
119 *A screen for mutants with altered adhesion*
120 The holdfast promotes adhesion of *C. crescentus* cells to a variety of surfaces(25). We reasoned
121 that adhesive cells could be depleted from liquid cultures by adding an attachment substrate with
122 a sufficiently large surface area. Cheesecloth has been used in this manner to enrich for holdfast
123 mutants in both *C. crescentus* and *Asticcacaulis biprosthecum,* another stalked bacterium in the
124 *Caulobacteraceae* clade(26, 27). Adding sterile cheesecloth to wild-type *C. crescentus* cultures
125 decreased the turbidity of the medium by titrating adhesive cells from the broth. This effect was
126 amplified in the hyper-adhesive Δ*hfiA* strain and not observed in the holdfast deficient Δ*hfsJ* strain
127 demonstrating the effectiveness of cheesecloth at capturing cells with a holdfast (Fig 1B). We
128 concluded that growth in the presence of cheesecloth could be used as the basis of a selection to
129 identify mutants defective in adhesion.
130 Saturating transposon mutagenesis coupled with transposon insertion sequencing (TnSeq)
131 offers the advantage of scoring phenotypes for all non-essential genes in the genome
132 simultaneously(28). Thus, combining TnSeq-based mutant profiling with cheesecloth depletion
133 seemed appropriate to perform a saturating screen for holdfast biosynthesis genes and identify

134 missing biosynthesis factors. We developed a randomly barcoded transposon library in *C.*
135 *crescentus* to enable the use of BarSeq(29) for profiling mutant fitness. Adhesive cells were
136 depleted by passaging the library in cheesecloth for five cycles. For each passage, the library was
137 cultured for 24-hours in the presence of cheesecloth after which the unattached cells in the
138 medium were used to re-inoculate a fresh culture containing cheesecloth. An aliquot of unattached
139 cells in the medium was also harvested for BarSeq analysis. Each passaging experiment was
140 performed in triplicate, and three parallel passaging experiments were also performed in medium
141 without cheesecloth to control for effects of mutation on growth rate (Table S2).

142 The abundance of each mutant during the passaging steps was assessed using BarSeq,
143 providing a temporal fitness profile for each gene over the course of the experiment(29). Genes
144 with higher fitness scores reflect mutants with adhesion defects that were enriched in medium
145 that had been depleted with cheesecloth. As expected most genes had inconsequential effects on
146 adhesion. However there were a significant number of genes whose mutation caused strong
147 cheesecloth dependent changes in abundance over the course of the multi-day experiment. The
148 250 genes with the highest fitness values, above or below the baseline level, are shown in Fig 1C.
149 The time resolved nature of the experiment allowed us to group mutants with similar fitness
150 profiles into distinct classes. Mutants with similar temporal adhesion profiles often mapped to
151 genes with similar or complementary annotations, indicating that they represented groups of
152 functionally related genes. We predicted the functions of uncharacterized genes using known
153 functions for genes with similar fitness profiles. For example, a cluster of genes whose mutants
154 show a continuous increase in abundance after each passage contains many known *hfs* genes, and
155 any uncharacterized genes that share this fitness profile would be predicted to contribute to
156 holdfast synthesis as well. We identified a total of four clusters containing mutants that display

157 distinct fitness profiles for the cheesecloth passaging experiment. Each cluster is described in
158 detail below.
159
160 *Mutants defective in smooth lipopolysaccharide display ectopic adhesion*
161 We identified a cluster of mutants with strong fitness decreases (i.e. increased adhesion to
162 cheesecloth) in early passages that recovered to near neutral or even positive fitness values as
163 passaging proceeded (Fig 2A). Many of the genes in this "recovery" cluster had annotations
164 associated with polysaccharide biosynthesis but had no known cellular function. However, the
165 *wbq* genes that are required for the production of smooth lipopolysaccharide (SLPS) comprised a
166 subset of the recovery cluster(30). This suggested that mutants sharing this fitness profile might
167 also be defective in the biosynthesis of SLPS.
168 We focused on three uncharacterized genes in the recovery cluster. *CCNA_00497* is
169 annotated as a putative rhamnosyl transferase, *CCNA_02386* is annotated as an O-antigen ligase
170 and *CCNA_03744* is homologous to *rfbB*, a gene required for the biosynthesis of dTDP-L-
171 rhamnose(31). Mutants in *CCNA_03744* were previously shown to suppress the holdfast
172 attachment defect observed in a Δ*hfaD* mutant, but SLPS was not examined in these cells(32). We
173 created in-frame deletions of *CCNA_00497*, *CCNA_02386* and *rfbB* and analyzed SLPS production by
174 immunoblotting. A deletion of *wbqP*, which is thought to encode the initial glycosyltransferase
175 step in the O-polysaccharide biosynthesis pathway, was used as a positive control. Disruption of
176 *CCNA_02386*, *rfbB* or *wbqP* led to the loss of detectable SLPS, while Δ*CCNA_00497* cells showed a
177 reduction in SLPS levels (Fig 2C). Additionally, all four mutants released the S-layer protein RsaA
178 into the spent medium, an additional hallmark of SLPS defects in *C. crescentus* (Fig 2C) (33). None
179 of the mutants displayed observable changes in rough LPS, demonstrating that they were not
180 defective in the production of lipid A or the core oligosaccharide (Fig S1). All of the defects could

181 be complemented by ectopic expression of the target gene, confirming their roles in the
182 production of SLPS (Fig 2C and Table S4).

183 The fitness profiles for early stages of cheesecloth passaging suggested that disrupting
184 SLPS led to hyper-adhesive cells that were rapidly depleted by cheesecloth. We chose to
185 investigate adhesion in detail using a defined medium because adhesion of wild-type cells is lower
186 in defined medium than in complex medium, making this condition better suited for detecting
187 increases in adhesion. We found that the SLPS mutants were indeed hyper-adhesive, producing CV
188 staining values ranging from 2 to 4 times that of wild type (Fig 2B). To understand the basis of
189 hyper-adhesion, Δ*wbqP* cells were imaged after staining with fluorescently labeled wheat germ
190 agglutinin (fWGA) to label holdfasts. Most wild-type cells displayed a fluorescent focus at the tip of
191 the stalk, and stalks from multiple cells often aggregated around a single focus to form rosette
192 structures that are characteristic of holdfast production. In the Δ*wbqP* background, a comparable
193 number of cells produced a holdfast, but the structure of the rosettes was altered. Cells that
194 assembled around a holdfast were more tightly packed, and not all of them adhered to the
195 aggregates through the tip of the stalk (Fig 2D).

196 The unusual rosette structures in the Δ*wbqP* mutant suggested that cells with disrupted
197 SLPS might have a second mode of adhesion that did not require holdfast. We compared fWGA
198 staining in the holdfast deficient Δ*hfsJ* strain to a Δ*hfsJ* Δ*wbqP* double mutant that lacks both
199 holdfast and SLPS. Δ*hfsJ* cells did not stain with fWGA and did not form aggregates. Δ*hfsJ* Δ*wbqP*
200 cells did not stain with fWGA, but in contrast to the Δ*hfsJ* strain, the cells still formed aggregates
201 (Fig 2D). These aggregates appeared not to be mediated by stalk-stalk interactions but rather
202 through interactions within the cell body. This further supported the idea that a holdfast-
203 independent mode of adhesion operates in SLPS mutants. Consistent with this model, bulk
204 adhesion in the Δ*hfsJ* Δ*wbqP* double mutant was not abolished, and was, in fact, higher than wild

205 type (Fig 2B). We conclude that disrupting SLPS production causes defects in the cell surface
206 leading to a holdfast independent mode of adhesion that represents the dominant mode of
207 adhesion for these mutants early in our experimental time course.
208
209 *The flagellum and type IV pili regulate holdfast production*
210 A second cluster of mutants displayed steady decreases in fitness throughout passaging in
211 cheesecloth. This group primarily contained genes known to participate in chemotaxis and
212 flagellar motility as well as components of the type IV pilus machinery. Thus, the data suggested
213 that disrupting the assembly of polar appendages, either pili or the flagellum, leads to hyper-
214 adhesion. To study the effects of polar appendages on adhesion, we deleted the genes for the
215 flagellar basal body component FlgH and the pilus assembly protein CpaH (34, 35). We confirmed
216 that Δ*flgH* showed the expected loss in motility and that Δ*cpaH* was resistant to the type IV pilus
217 specific phage ΦCBK (Figs S2 and S3).
218 Both the Δ*flgH* and the Δ*cpaH* mutants showed adhesion defects in complex medium (Table
219 S4). However, in defined medium, both mutants displayed increased adhesion relative to wild
220 type, indicating that disrupting the pilus or the flagellum causes hyper-adhesion under these
221 conditions (Fig 3B). To reconcile these differences we used fWGA staining to measure the
222 proportion of cells that produced a holdfast. The Δ*flgH* and Δ*cpaH* mutants produced more
223 holdfasts than wild-type in both complex and defined medium (Fig S3 and Table S6). We conclude
224 that flagellum and pilus mutations increase holdfast production, but that loss of either appendage
225 also leads to holdfast-independent defects in surface colonization. Pili and flagella often have
226 similar effects on surface colonization in other systems(36, 37). Because the baseline level of
227 holdfast production is low in defined medium, the enhanced holdfast production Δ*flgH* and Δ*cpaH*
228 backgrounds appears to outweigh surface colonization defects under these conditions (Fig S3).

229 A recent report showed that flagellar hook mutants displayed decreased transcription from
230 the *hfiA* promoter (P_{hfiA}) in defined medium and that this effect did not occur in the absence of the
231 diguanylate cyclase PleD(38-40). This led us to examine the relationships between our polar
232 appendage mutants, *hfiA* and *pleD*. We used a P_{hfiA}-*lacZ* reporter to measure transcription from the
233 *hfiA* promoter. Because expression from P_{hfiA} is nearly undetectable in complex medium, we
234 focused on transcriptional changes that occurred in defined medium. The Δ*flgH* and Δ*cpaH*
235 mutants showed reduced *hfiA* transcription in the reporter assay (Fig 3D). These effects were
236 abrogated in the Δ*flgH* Δ*pleD* and Δ*cpaH* Δ*pleD* double mutants (Fig 3D). Likewise, bulk adhesion
237 in defined medium reverted to near wild-type levels in the Δ*flgH* Δ*pleD* and Δ*cpaH* Δ*pleD* mutants,
238 confirming that *pleD* contributes to the modulation of P_{hfiA} caused by pilus and flagellar mutants
239 (Fig 3C). We note, however, that a full reversion of the hyper-holdfast phenotype would be
240 predicted to display bulk adhesion levels below that of wild type due to the holdfast-independent
241 attachment defects seen in pilus and flagellar mutant backgrounds. Thus, while *pleD* does
242 contribute to the enhanced adhesion seen in the Δ*flgH* and Δ*cpaH* mutants, the effect is not
243 completely dependent on this gene.

244 To test whether the hyper-adhesive phenotypes in the polar appendage mutants could be
245 explained by regulation of *hfiA,* we created Δ*flgH* Δ*hfiA* and Δ*cpaH* Δ*hfiA* double mutants. Though
246 Δ*flgH* Δ*hfiA* cells remained hyper-adhesive in defined medium, bulk attachment was not
247 significantly increased relative to the Δ*flgH* single deletion. This suggests that Δ*flgH* minimizes the
248 effects of *hfiA*, and that holdfast-independent adhesion defects lower the maximum level of CV
249 staining that can be achieved in a Δ*flgH* background. The enhanced attachment seen in the Δ*cpaH*
250 background was further increased in a Δ*cpaH* Δ*hfiA* double mutant ($P < 0.0001$; Fig 3C). Thus,
251 Δ*cpaH* has an intermediate effect on *hfiA* activity by dampening but not completely masking its
252 activity. Consistent with this, the percentage of Δ*cpaH* cells that produced a holdfast in defined

253 medium was intermediate between that of wild type and Δ*hfiA*, supporting the idea that Δ*cpaH*
254 causes both intermediate enhancement of holdfast production and holdfast-independent surface-
255 attachment defects (Fig S3 and Table S6). Finally, bulk adhesion in a Δ*flgH* Δ*cpaH* double mutant
256 was indistinguishable from Δ*flgH*, and P_{hfiA} transcription was lower in Δ*flgH* Δ*cpaH* than either the
257 Δ*flgH* ($P < 0.0001$) or Δ*cpaH* ($P < 0.0001$) single mutants (Fig 3B and C). This result indicates that
258 holdfast production is likely maximized in the Δ*flgH* mutant and that the Δ*flgH* and Δ*cpaH* mutants
259 modulate P_{hfiA} through separate pathways.
260
261 *A complex role for the pilus in regulating adhesion*
262 The Δ*cpaH* phenotype suggested that disrupting pilus assembly leads to increased holdfast
263 production via the repression of *hfiA*. However, a closer examination of the fitness profiles for
264 genes involved in type IV pilus assembly revealed a range of phenotypes for various components
265 of the apparatus (Fig 4A). Mutants in most of the genes encoding components of the pilus
266 secretion machinery, including *cpaH,* showed decreased fitness scores consistent with hyper-
267 adhesion. However, mutations in the gene coding for the main pilin subunit, PilA, displayed the
268 opposite trend. *pilA* mutants showed an increase in fitness during passaging in cheesecloth that
269 would be expected for mutants with adhesion defects. We confirmed that, indeed, the Δ*pilA* strain
270 was defective in surface attachment both in complex and defined medium (Fig 4B and Table S4).
271 To examine the relationship between *pilA*-dependent loss of adhesion and the activation of
272 adhesion observed in mutants that disrupt pilus and flagellum assembly we created Δ*flgH* Δ*pilA*
273 and Δ*cpaH* Δ*pilA* double mutants. The phenotypes for these mutants were similar in both complex
274 and defined medium (Table S5). Surface attachment levels in the Δ*flgH* Δ*pilA* mutant were
275 intermediate to those of Δ*pilA* ($P < 0.0001$) and Δ*flgH* ($P < 0.0001$), suggesting that *flgH* and *pilA*
276 regulate adhesion through independent, additive pathways (Fig 4C and Table S5). In contrast,

277 adhesion in the Δ*cpaH* Δ*pilA* mutant was indistinguishable from Δ*pilA* demonstrating that the
278 effects of *pilA* on adhesion are epistatic to those of *cpaH* (Fig 4C and Table S5). We conclude that
279 the pilin subunit PilA is required for the holdfast promoting effect caused by disruption of the
280 pilus assembly apparatus.

281 We further explored the model that *pilA* contributed to the modulation of adhesion by *cpaH*
282 by examining the relationships between *pilA, hfiA* and *pleD*. The decreased adhesion observed in
283 the Δ*pilA* mutant was not reversed in a Δ*pilA* Δ*pleD* background indicating that the effect of *pilA* on
284 adhesion is *pleD*-independent. Adhesion in a Δ*pilA* Δ*hfiA* double mutant was elevated to a level
285 slightly below that of the Δ*hfiA* strain ($P < 0.0001$; Fig 4B). The difference in surface attachment
286 between the Δ*pilA* Δ*hfiA* and Δ*hfiA* mutants likely reflects the holdfast-independent surface
287 attachment defects caused by the loss of a functional pilus. Expression from P_{hfiA} was only slightly
288 elevated in the Δ*pilA* mutant (Fig 4D). Because *hfiA* is already highly expressed under these
289 conditions, it is difficult to determine if P_{hfiA} is activated further in the Δ*pilA* mutant. Finally, β-
290 glactosidase activity from the P_{hfiA} reporter in both the Δ*flgH* Δ*pilA* and Δ*cpaH* Δ*pilA* backgrounds
291 was restored to wild-type levels demonstrating that Δ*pilA* blocks *hfiA* activation in the Δ*flgH* and
292 Δ*cpaH* backgrounds (Fig 4D).

293

294 *New factors in the holdfast biosynthesis pathway*

295 The final two clusters of mutants presented in Fig 1C displayed a continuous increase in fitness
296 during growth in cheesecloth that would be predicted for mutants with adhesion defects. We used
297 the magnitude of the measured fitness increases to separate these genes into *1)* a cluster with
298 higher fitness scores that contained all of the *hfs* genes known to be required for robust adhesion
299 and *2)* a cluster displaying more modest fitness increases which contained the *hfsK* gene. *hfsK*
300 codes for an enzyme thought to modify the holdfast polysaccharide in order to produce a fully

301 adhesive holdfast(24). We chose three uncharacterized genes from these clusters of mutants to
302 examine in detail for holdfast defects.

303 Disruption of *CCNA_01242,* which encodes a predicted amino acid permease, leads to the
304 highest fitness increase of any gene in the cheesecloth passaging experiment (Fig 5A). However,
305 the Δ*CCNA_01242* strain had only a modest defect in surface attachment (Fig 5B). There were no
306 obvious holdfast defects in the mutant and we could not detect a significant adhesion defect under
307 any conditions tested (Fig 5C and Table S4). Δ*CCNA_01242* had an unusual, biphasic growth
308 profile. In complex medium, log phase was shorter than wild type, leading to a lower optical
309 density as growth began to slow prematurely. Growth of this strain continued slowly over the next
310 24 hours and eventually plateaued at a similar optical density to wild type (Fig S4). The biphasic
311 growth likely confounds fitness calculations for samples collected during the sequential passaging
312 experiment. It is not clear why *CCNA_01242* mutants were more enriched when cheesecloth was
313 included in the medium, but we conclude nonetheless that the gene does not contribute to holdfast
314 production.

315 *CCNA_02360* is a predicted member of the GT2 family of glycosyltransferases. Its
316 disruptions have a fitness profile closely resembling many of the known *hfs* genes (Fig 5A). A
317 Δ*CCNA_02360* mutant was non-adhesive in CV staining assays and did not stain with fWGA under
318 any conditions tested (Figs 5B and 5C). Given the lack of holdfast production in Δ*CCNA_02360*
319 cells, we predict that *CCNA_02360* encodes a glycosyltransferase that contributes one or more
320 monosaccharides to repeating unit of the holdfast polysaccharide and have named this gene *hfsL.*
321 Previous studies have mentioned mutants in *CCNA_02360* as a holdfast-deficient control strain(24,
322 39), but, curiously, the identification of the gene and characterization of its phenotype have not
323 been reported. Closely related genes could be identified in many stalked bacteria within the
324 *Caulobacterales* clade suggesting that HfsL carries out a conserved step in holdfast biosynthesis.

325 Identifying close homologs in more distantly related *Alphaproteobacteria* was difficult due to the
326 abundance of GT2 family glycosyltransferases in bacterial genomes. Nevertheless, HfsL represents
327 a fourth glycosyltransferase that is required for holdfast biosynthesis in *C. crescentus.*

328 *CCNA_02722* is a hypothetical protein that does not show homology to any known protein
329 families. It has a predicted N-terminal signal peptide for export to the periplasm. The fitness
330 profile is similar to *hfsK,* showing a modest increase in fitness during passaging in cheesecloth
331 suggestive of intermediate defects in adhesion (Fig 5A). The Δ*CCNA_02722* mutant was
332 significantly in impaired surface-attachment (Fig 5B). When planktonic Δ*CCNA_02722* cells were
333 stained with fWGA, holdfast staining was apparent (Fig 5C). However, using adhesion assays in
334 which cells are grown in the presence of a glass slide that is then washed, stained with fWGA and
335 imaged we detected a holdfast attachment defect. Wild-type cells normally coat the surface of the
336 slide and show fWGA foci at the site of attachment, but we observed very few attached
337 Δ*CCNA_02722* cells. Instead, the slide was coated with an abundance of fWGA reactive material
338 (Fig 5C). This holdfast shedding phenotype is characteristic of mutants with defects in attaching
339 the holdfast matrix to the surface of the stalk(27), and the gene has been named *hfaE* accordingly.
340 Like *hfsL, hfaE* could be identified in the genomes of many other stalked bacteria suggesting a
341 conserved role in holdfast attachment.

342

343 **Discussion**

344 Holdfast production in *C. crescentus* presents an attractive model system to interrogate the
345 assembly of polysaccharides in bacteria. Lectin staining, enzymatic sensitivity and functional
346 annotations for the *hfs* genes indicate that the holdfast contains a polysaccharide(16, 17, 22).
347 However, despite decades of work, surprisingly little else is known about the chemical structure of
348 the holdfast. As part of our efforts to characterize the biosynthetic pathway, we sought a complete

349 list of enzymes required for holdfast biosynthesis. In order to saturate the search for *hfs* genes, we
350 developed a TnSeq-based method to measure the adhesion phenotype conferred by each non-
351 essential gene in the genome.

352 The genome-wide approach provided a surprisingly rich set of insights into adhesion in *C.*
353 *crescentus.* Not only did the screen identify non-adhesive mutants representing missing
354 components of the holdfast pathway, but it also resolved mutants that displayed increased
355 adhesion. One class of such mutants was defective in the production of smooth-LPS. Disrupting
356 SLPS resulted in elevated adhesion levels in both holdfast producing and holdfast deficient
357 backgrounds. SLPS mutants no longer adhered exclusively at the stalks of holdfast producing cells,
358 but rather displayed a generalized form adhesion throughout the cell surface. Our analysis of these
359 mutants supports a model in which the *C. crescentus* envelope is structured to ensure that the cell
360 surface is non-adhesive, maximizing the opportunity for polar adhesion via the holdfast.

361 A holdfast independent form of adhesion could explain the unexpected fitness profiles seen
362 in SLPS mutants during passaging in cheesecloth. The unique mode of aggregation conferred by
363 having both a holdfast and a disrupted cell surface clearly leads to an initial depletion of these
364 mutants from the culture medium by cheesecloth. However, as non-adhesive *hfs* mutants begin to
365 dominate the culture, this adhesion strategy may lose its effectiveness, leading to a recovery
366 phase. Regardless of mechanism, our analysis allowed for the identification of new SLPS
367 biosynthesis genes in *C. crescentus* simply by defining a group of mutants that shared the
368 characteristic depletion and recovery profile over the course of the passaging experiment. Such
369 co-fitness approaches have been useful in other contexts(41) and allowed us to greatly expand the
370 number of genes in the *C. crescentus* SLPS pathway (Table S3).

371 Genes with predicted functions in motility, flagellar biosynthesis and type IV pilus
372 assembly displayed a hyper-adhesive profile that could be distinguished from SLPS mutants by the

373 lack of a recovery phase. Mutations in components of the flagellar basal body were recently shown
374 to enhance holdfast production by inhibiting the expression of *hfiA,* a result that we confirmed
375 here in our examination of *flgH*(40). Co-fitness analysis indicated that the *cpa* genes, which code
376 for components of the type IV pilus, have a similar phenotype, and we showed that mutating the
377 inner-membrane pilus assembly component *cpaH* also increased holdfast production by
378 repressing *hfiA*. However, mutating *pilA,* which codes for the main subunit of the pilus filament,
379 reduced adhesion. The adhesion defect in Δ*pilA* cells was partially restored in a Δ*pilA* Δ*flgH*
380 background but remained unchanged in Δ*pilA* Δ*cpaH* cells. Thus, although the Δ*flgH* and Δ*cpaH*
381 mutations both enhance holdfast production, the two pathways can be distinguished by their
382 requirement for *pilA*. Disentangling the specific routes by which the various polar appendage
383 mutants modulate *hfiA* activity will require identifying intermediate factors in the signaling
384 pathways, but our results underscore the interconnectedness of the flagellum, pilus and holdfast.

385 Numerous reports have debated the roles of pili and the flagellum in surface
386 attachment(12-14, 42, 43). Our unbiased, genome-wide analysis of adhesion unambiguously
387 identified both appendages as determinants of attachment. Two recent studies, in particular,
388 showed that mutating the flagellar basal body represses *hfiA* and that disruption of flagellar
389 rotation upon surface contact stimulates holdfast production(14, 40). In our cheesecloth
390 passaging experiment flagellar motor (*mot*), flagellin glycosylation (*flm)* and chemotaxis (*che*)
391 genes shared the same hyper-adhesive fitness profile as components of the flagellar basal body
392 (Table S3). Some of these mutants would be predicted to disrupt flagellar rotation without
393 affecting assembly *per se*(44). We propose that disrupting flagellar function, either through
394 physical interaction with a surface or mutation of motility genes, stimulates holdfast production. It
395 will be interesting to test this model by determining whether the repression of *hfiA* seen in the
396 flagellar mutants is required to activate holdfast production after surface contact. We also note

397 that future studies should take into account the finding that mutating *flgH* reduces biofilm
398 formation in a holdfast-independent manner (Fig S3), suggesting flagellar motility likely also
399 promotes productive interactions with a surface that lead to permanent attachment.

400 Much like flagellar mutants, disrupting components of the type IV pilus also causes both
401 increased holdfast production and holdfast-independent surface colonization defects. A recent
402 report proposed that contact with a surface inhibits the retraction of PilA filaments leading to a
403 stimulation of holdfast production(13). One might initially conclude that pilus assembly defects in
404 the *cpa* mutants mimic the obstruction of pilus filament oscillation. However, the situation is more
405 complex because *pilA* was required for increased holdfast production in the Δ*cpaH* mutant. These
406 findings can be reconciled in a model in which the disruption of filament oscillation caused either
407 by surface contact or upon mutation of the *cpa* genes leads to changes in the PilA pool that serve
408 as a signal to stimulate holdfast production. A similar model was proposed for the regulation of
409 biofilm formation by the *Agrobacterium tumefaciens* pilus(37). Again, determining if repression of
410 *hfiA* is required for the induction of holdfast production upon surface contact would help to clarify
411 whether the *hfiA*-dependent and surface stimulated pathways are one in the same.

412 Finally, the initial goal of this study was to saturate the search for holdfast production
413 factors. We used the cheesecloth passages to define a temporal fitness profile that was shared by
414 genes known to be required for holdfast biosynthesis and used this pattern to search for missing
415 genes in the pathway. In addition to a new holdfast attachment factor (*hfaE*), we identified a
416 glycosyltransferase (*CCNA_02360*), which we have named *hfsL*, and showed that it is required for
417 holdfast production. Due to the saturating nature of our experiment, we believe that HfsE (along
418 with the redundant PssY and PssZ), HfsJ, HfsG and HfsL carry out the only four glycosyltransferase
419 steps involved in holdfast biosynthesis. Thus, we predict that a repeating unit of four or more
420 monosaccharides makes up the holdfast polysaccharide because each of these enzymes likely

421 contributes at least one sugar to the glycolipid intermediate that serves as a substrate for
422 polymerization.

423 Implicit in defining the complete set of genes in the holdfast pathway is knowledge of genes
424 that do not contribute. Many bacterial polysaccharides contain specialized monosaccharide
425 components(45, 46). Such intermediates are synthesized as nucleotide activated precursors that
426 can be directly utilized by glycosyltransferases(47, 48). We did not identify any genes involved in
427 nucleotide sugar metabolism that had significant adhesion defects when disrupted. This suggests
428 that the holdfast does not contain specialized monosaccharide components but is instead
429 composed of "housekeeping" sugars that are shared by other cellular processes. Such insights into
430 the nature of the sugar components will help inform our ongoing efforts to characterize the
431 chemical structure of the holdfast polysaccharide. Additionally, the ability to utilize standard
432 nucleotide sugars as substrates without requiring specialized chemical syntheses will make the
433 holdfast biosynthetic enzymes useful models for probing the catalytic mechanisms of bacterial
434 polysaccharide biosynthesis.

435 More broadly, the findings reported here highlight the advantages to probing mutant
436 phenotypes in parallel. Classical genetic selections in which mutants are enriched then isolated
437 and analyzed separately inherently favor both the most extreme phenotypes and large genes that
438 have the highest likelihood of acquiring mutations. Screening pools of mutants in parallel using
439 TnSeq eliminates these biases, allowing detection of a range of phenotypes and analysis of
440 mutations in short genes that represent a small fraction of the mutant pool. In this study, we
441 discovered new regulatory networks that modulate holdfast synthesis by identifying mutants that
442 display modest adhesion increases using a genetic background in which cells are already adhesive.
443 Such mutants would be extremely difficult to isolate using a classical approach. Additionally, the
444 saturating nature of these experiments makes them ideal for outlining complete biosynthetic

445 pathways. Having a reasonable measure of completeness allowed us to leverage the results of the
446 genome-wide screen to propose a model for the enzymatic steps in the holdfast pathway that will
447 inform efforts to reconstitute the biosynthetic reactions *in vitro* (Fig 6).
448
449 **Methods**
450 *Strains, growth conditions and genetic manipulation*
451 Strains and plasmids used in this study are listed in Table S1. *E. coli* strains were grown in LB at
452 37°C with diaminopimelic acid (60 mM), kanamycin (50 μg/mL) or tetracycline (12 μg/mL)
453 included as needed. *C. crescentus* CB15 was grown either in PYE (complex) or M2 salts containing
454 0.15% xylose (M2X, defined) at 30°C (49). When necessary sucrose (3%), kanamycin (25 μg/mL)
455 or tetracycline (2 μg/mL) was included in solid medium. Kanamycin (5 μg/mL) or tetracycline (1
456 μg/mL) was included in liquid medium when necessary. Standard techniques were used for
457 cloning and sequencing plasmids. Plasmids were introduced by electroporation or, in the case of
458 the pFC1948 reporter plasmid, by tri-parental mating. Unmarked mutations were created
459 through two-step deletion using a SacB counter-selection. Mutants were complemented by
460 inserting target genes into pMT585, which allows for the integration of the gene at the *xyl* locus
461 under the transcriptional control of P_{xyl}(50). When necessary, target genes were inserted into
462 pMT585 in reverse orientation under the control of their native promoters.
463
464 *Library development and mapping*
465 The barcoded HiMar transposon pool APA_752 developed by Wetmore et al.(29) was used to
466 create a barcoded Tn library in *C. crescentus*. Construction of the library has been reported
467 previously along with its associated statistics(51). Briefly, the transposon pool was introduced
468 into *C. crescentus* by conjugation. Transconjugants appearing on selective plates were pooled, used

469 to inoculate a liquid culture with Kanamycin and grown for 3 doublings. Glycerol was added to a
470 final concentration of 15% and 1mL aliquots were frozen and stored at -80°C. TnSeq also followed
471 the method of Wetmore et al(29). A 1mL library aliquot was centrifuged and genomic DNA was
472 extracted from the pellet. The DNA was sheared, size selected for ~300bp fragments and end
473 repaired. A custom Y-adapter (Mod2_TS_Univ annealed to Mod2_TruSeq) was ligated and
474 transposon junctions were amplified by PCR using the Nspacer_BarSeq_pHIMAR and
475 P7_mod_TS_index1 primers. An Illumina HiSeq2500 was used to generate 150bp single-end reads
476 of the library. The genomic positions of were determined with BLAT. The barcode corresponding
477 to each insertion site was determined using MapTnSeq.pl. This information was used to develop a
478 list of barcodes that mapped to unique insertion sites using DesignRandomPool.pl (available at
479 https://bitbucket.org/berkeleylab/feba).
480
481 *Passaging in cheesecloth*
482 1 mL aliquots of the DH1 transposon library was thawed at room temperature and 300 µL of the
483 library was inoculated into a well of a12-well microtiter plate containing 1.2 mL PYE and a stack of
484 5 ~10 mm x 10 mm squares of sterile cheesecloth was added. The culture was grown with 155
485 rpm shaking at 30°C for 24 hours after which 100 µL of the planktonic culture was used to
486 inoculate a fresh well containing 1.4 mL PYE and a fresh piece of sterile cheesecloth. An additional
487 500 µL of the planktonic culture medium was centrifuged and the pellet was stored at -20°C for
488 BarSeq analysis. The process was repeated for a total of five passages and each passaging
489 experiment was performed in triplicate. The same procedure was used to perform passaging
490 experiments in which no cheesecloth was added.
491
492 *Fitness determination with BarSeq*

493 Cell pellets from 0.5mL of planktonic culture medium that had been frozen after each passage
494 were used as templates for PCR reactions that simultaneously amplified the barcode region of the
495 transposons while adding TruSeq indexed Illumina adaptors(29). The PCR products were purified,
496 pooled and multiplexed on a single Illumina 4000 lane for sequencing. Fitness values for each gene
497 were determined using the pipeline described by Wetmore et al(29). Barcodes for each read were
498 mapped using MultiCodes.pl and correlated with their associated insertion positions using
499 combineBarSeq.pl. This data was used to calculate fitness using FEBA.R. This analysis determines
500 strain fitness as the $\log_2$ ratio of barcode counts in a sample to the barcode counts in the reference
501 condition, for which we used the first passage of the library in PYE without cheesecloth. Gene
502 fitness was calculated by determining the weighted average of the insertion mutants with a given
503 gene, excluding the first and last 10% of the ORF. The scripts used for fitness determination can be
504 found at https://bitbucket.org/berkeleylab/feba.
505
506 *Data availability*
507 The raw sequence data for each BarSeq sample along with a table describing the barcode
508 abundances and their genomic insertion sites has been uploaded to the NCBI Gene Expression
509 Omnibus (GEO) at https://www.ncbi.nlm.nih.gov/geo/ under the accession: GSE119738.
510
511 *Analysis of fitness data*
512 We focused on identifying genes with the highest absolute (positive or negative) fitness scores.
513 For each passaging step (with and without cheesecloth), an average and a standard deviation for
514 the three replicate samples were calculated. Genes for which the largest standard deviation across
515 the ten passages was greater than the largest absolute fitness score were eliminated from further
516 analysis. Fitness scores determined for each passage without cheesecloth were subtracted from

517 those of the corresponding passage with cheesecloth to normalize for growth defects. These
518 normalized values were used to rank each gene according to its largest absolute fitness score at
519 any stage of cheesecloth passaging. The top 250 genes were then sorted by hierarchical
520 clustering(52) to identify genes with related fitness patterns. Groups derived from the clustering
521 analysis were curated manually to produce the genes in Tables S4-S8.
522
523 *Crystal violet (CV) staining of adherent cells*
524 Saturated cultures of *C. crescentus* grown in PYE were diluted to OD_{660}=0.4 with PYE, 1uL was
525 inoculated into the wells of 48-well microtiter plates containing 450uL medium and the cultures
526 were shaken for 24 hours. For cultures used to measure the effects of motility mutants on
527 adhesion, the incubation was shortened to 17 hours. The cultures were then discarded and the
528 plates were washed thoroughly with a steady stream of tap water. The wells were stained for 5
529 min with 0.01% crystal violet and washed again with tap water. Stain was dissolved for 5 min in
530 100% EtOH and quantified by reading absorbance at 575nm.
531
532 *Fluorescent wheat germ agglutinin (fWGA) staining*
533 For staining of planktonic cells, 400 µL of liquid culture was added to an Eppendorf tube and
534 Alexa594 conjugated-WGA (ThermoFisher) was added to a final concentration 0.5 mg/mL. After
535 incubating the cells for 5 min in the dark, 1mL of sterile water was added and the cells were
536 centrifuged at 6k x g for 2 min. The pellet was re-suspended in 5 µL of medium, spotted on a glass
537 slide and imaged. Cells were imaged with a Leica DM500 microscope equiped with a HCX PL APO
538 63X/ 1.4na Ph3 objective. fWGA staining was visualized using an RFP fluorescence filter (Chroma
539 set 41043). For quantifying the number of holdfast-producing cells, a culture was inoculated to an

540 OD_{660} of 0.002 and harvested when the OD_{660} reached 0.05-0.1 to minimize the number of
541 rosettes.
542 For staining attached cells, a glass coverslip was washed with ethanol and added to a 1mL
543 PYE culture of the appropriate strain in a 12-well plate. The cultures were grown for 6-8hrs. Un-
544 attached cells were removed from the coverslip by washing under a stream of distilled water. One
545 side of the glass was covered with a solution of 0.5 mg/mL fWGA in PYE, incubated for 5 min in the
546 dark and washed under a stream of distilled water. The coverslip was placed stain side down on a
547 glass slide and imaged with phase contrast and fluorescence as described above.
548
549 *Smooth lipopolysaccharide (SLPS) Immunoblotting*
550 Lysates for immunoblotting were prepared by the method of Walker et al(53). Pellets from
551 saturated cultures were treated with DNAse and lysozyme, mixed with SDS-running buffer and
552 digested with proteinase K. Samples were separated on a Tris-glycine SDS-PAGE gel with 12%
553 acrylamide and transferred to nitrocellulose. The amount of sample loaded was normalized to the
554 final optical density of the culture at harvest. The membrane was blocked in 5% milk, probed with
555 a 1 in 20,000 dilution of anti-SLPS serum raised in rabbit, washed, probed with HRP-conjugated
556 goat-anti-rabbit antibody, washed again and visualized with peroxidase substrate(33). The top
557 half of the membrane was removed before blocking and stained with Ponceau S as a loading
558 control.
559
560 *Analysis of Rough LPS*
561 LPS was extracted by the method of Darveau and Hancock(54). Cells were isolated from saturated
562 50mL *C. crescentus* cultures grown in M2X by centrifugation, re-suspended in 2 mL of 10 mM Tris-
563 HCl pH 8.0 containing 2 mM $MgCl_2$, and sonicated. DNAseI and RNAseA were added to 100 μg/mL

564 and 25 μg/mL, respectively and the lysate was incubated for 1 hour at 37°C. Additional DNAseI
565 and RNAseA were added to 200 μg/mL and 50 μg/mL, respectively and the lysate was incubated
566 for an additional 1 hour at 37°C. SDS and EDTA were added to 2% and 100 mM, respectively, and
567 the lysate was incubated for 2 hours at 37°C. The solution was then centrifuged for 30 min at
568 50,000 x *g*. Proteinase K was added to 50 μg/mL in the supernatant and the solution was
569 incubated for 2 hours at 60°C after which the LPS was precipitated with 2 volumes of ice-cold
570 0.375 M $MgCl_2$ in 95% EtOH and collected by centrifugation at 12,000 x *g*. The precipitate was re-
571 suspended in 2% SDS containing 100mM EDTA, incubated overnight at 37°C, and re-precipitated
572 with 0.375 M $MgCl_2$ in 95% EtOH. The precipitate was then suspended in 10 mM Tris-HCl pH 8.0
573 and centrifuged for 2 hours at 200,000 x *g*. The LPS pellets from each strain were suspended in
574 SDS loading dye and separated on by Tris-Tricine SDS-PAGE on an 18% acrylamide gel containing
575 6M urea. LPS was stained using the periodate-silver method of Kittelberger and Hilbink(55).
576
577 *Bacteriophage ΦCBK sensitivity*
578 Saturated cultures of *C. crescentus* grown in PYE were diluted to OD_{660}=0.4 with PYE, serially
579 diluted and spotted on PYE plates containing 0.15% xylose that had been spread with $1*10^{-7}$
580 PFU/mL ΦCBK or PYE plates with 0.15% xylose alone. The plates were incubated for 48hrs at
581 30°C and photographed.
582
583 *Soft-agar swarming assay*
584 Saturated cultures of *C. crescentus* grown in PYE were spotted in plates of PYE containing 0.3%
585 agar and 0.15% xylose. The plates were incubated for 4 days at 30°C and photographed.
586
587 *lacZ reporter assay*

588 Cultures for measuring reporter activity were grown in M2X medium and the amount of culture
589 required to achieve an OD_{660} of 0.0005-0.00075 was added to fresh M2X medium. These cultures
590 were grown to an OD_{660} of 0.05-0.15 and β-galactosidase activity was measured as previously
591 described(10).

592 **Acknowledgements**

593 We thank members of the Crosson lab and Prof. Arash Komeili for helpful discussions and insight.
594 This work was supported by NIH grant R01GM087353 to S.C. D.M.H. is supported by the Helen
595 Hay Whitney Foundation.

596

597 **References**

598 1. **Silhavy TJ**, **Kahne D**, **Walker S**. 2010. The Bacterial Cell Envelope. Cold Spring Harbor
599 Perspectives in Biology **2**:a000414–a000414.

600 2. **Whitfield C**. 2006. Biosynthesis and Assembly of Capsular Polysaccharides in Escherichia
601 coli. Annu Rev Biochem **75**:39–68.

602 3. **Joiner KA**. 1988. Complement evasion by bacteria and parasites. Annu Rev Microbiol
603 **42**:201–230.

604 4. **Roberson EB**, **Firestone MK**. 1992. Relationship between Desiccation and
605 Exopolysaccharide Production in a Soil Pseudomonas sp. Appl Environ Microbiol **58**:1284–
606 1291.

607 5. **Geno KA**, **Gilbert GL**, **Song JY**, **Skovsted IC**, **Klugman KP**, **Jones C**, **Konradsen HB**, **Nahm**
608 **MH**. 2015. Pneumococcal Capsules and Their Types: Past, Present, and Future. Clin
609 Microbiol Rev **28**:871–899.

610 6. **Whitfield C**. 2010. Polymerases: Glycan chain-length control. Nat Chem Biol **6**:403–404.

611 7. **Poindexter JS**. 1964. Biological properties and classification of the *Caulobacter* group.
612 Bacteriol Rev **28**:231–295.

613 8. **Degnen ST**, **Newton A**. 1972. Chromosome replication during development in Caulobacter
614 crescentus. J Mol Biol **64**:671–680.

615 9. **Henrici AT**, **Johnson DE**. 1935. Studies of Freshwater Bacteria: II. Stalked Bacteria, a New
616 Order of Schizomycetes. J Bacteriol **30**:61–93.

617 10. **Fiebig A**, **Herrou J**, **Fumeaux C**, **Radhakrishnan SK**, **Viollier PH**, **Crosson S**. 2014. A Cell
618 Cycle and Nutritional Checkpoint Controlling Bacterial Surface Adhesion. PLoS Genet
619 **10**:e1004101–14.

620 11. **Purcell EB**, **Siegal-Gaskins D**, **Rawling DC**, **Fiebig A**, **Crosson S**. 2007. A photosensory
621 two-component system regulates bacterial cell attachment. Proc Natl Acad Sci U S A
622 **104**:18241–18246.

623 12. **Li G**, **Brown PJB**, **Tang JX**, **Xu J**, **Quardokus EM**, **Fuqua C**, **Brun YV**. 2011. Surface contact
624 stimulates the just-in-time deployment of bacterial adhesins. Mol Microbiol **83**:41–51.

625 13. **Ellison CK**, **Kan J**, **Dillard RS**, **Kysela DT**, **Ducret A**, **Berne C**, **Hampton CM**, **Ke Z**, **Wright**
626 **ER**, **Biais N**, **Dalia AB**, **Brun YV**. 2017. Obstruction of pilus retraction stimulates bacterial
627 surface sensing. Science **358**:535–538.

628 14. **Hug I**, **Deshpande S**, **Sprecher KS**, **Pfohl T**, **Jenal U**. 2017. Second messenger–mediated
629 tactile response by a bacterial rotary motor. Science **358**:531–534.

630 15. **Kurtz HD Jr**, **Smith J**. 1992. Analysis of a Caulobacter crescentus gene cluster involved in
631 attachment of the holdfast to the cell. J Bacteriol **174**:687–694.

632 16. **Smith CS**, **Hinz A**, **Bodenmiller D**, **Larson DE**, **Brun YV**. 2003. Identification of Genes
633 Required for Synthesis of the Adhesive Holdfast in Caulobacter crescentus. J Bacteriol
634 **185**:1432–1442.

635 17. **Toh E**, **Kurtz HD**, **Brun YV**. 2008. Characterization of the Caulobacter crescentus Holdfast
636 Polysaccharide Biosynthesis Pathway Reveals Significant Redundancy in the Initiating
637 Glycosyltransferase and Polymerase Steps. J Bacteriol **190**:7219–7231.

638 18. **Wan Z**, **Brown PJB**, **Elliott EN**, **Brun YV**. 2013. The adhesive and cohesive properties of a
639 bacterial polysaccharide adhesin are modulated by a deacetylase. Mol Microbiol **88**:486–
640 500.

641 19. **Samuel G**, **Reeves P**. 2003. Biosynthesis of O-antigens: genes and pathways involved in
642 nucleotide sugar precursor synthesis and O-antigen assembly. Carbohydr Res **338**:2503–
643 2519.

644 20. **Islam ST**, **Lam JS**. 2014. Synthesis of bacterial polysaccharides via the Wzx/Wzy-dependent
645 pathway. Can J Microbiol **60**:697–716.

646 21. **Hong Y**, **Reeves PR**. 2014. Diversity of O-Antigen Repeat Unit Structures Can Account for
647 the Substantial Sequence Variation of Wzx Translocases. J Bacteriol **196**:1713–1722.

648 22. **Merker RI**, **Smit J**. 1988. Characterization of the adhesive holdfast of marine and freshwater
649 caulobacters. Appl Environ Microbiol **54**:2078–2085.

650 23. **Hernando-Pérez M**, **Setayeshgar S**, **Hou Y**, **Temam R**, **Brun YV**, **Dragnea B**, **Berne C**.
651 2018. Layered Structure and Complex Mechanochemistry Underlie Strength and Versatility
652 in a Bacterial Adhesive. mBio **9**:e02359–17–19.

653 24. **Sprecher KS**, **Hug I**, **Nesper J**, **Potthoff E**, **Mahi M-A**, **Sangermani M**, **Kaever V**, **Schwede**
654 **T**, **Vorholt J**, **Jenal U**. 2017. Cohesive Properties of the *Caulobacter crescentus* Holdfast
655 Adhesin Are Regulated by a Novel c-di-GMP Effector Protein. mBio **8**:e00294–17–15.

656 25. **Berne C**, **Ma X**, **Licata NA**, **Neves BRA**, **Setayeshgar S**, **Brun YV**, **Dragnea B**. 2013.
657 Physiochemical Properties of Caulobacter crescentusHoldfast: A Localized Bacterial
658 Adhesive. J Phys Chem B **117**:10492–10503.

659 26. **Umbreit TH**, **Pate JL**. 1978. Characterization of the holdfast region of wild-type cells and
660 holdfast mutants of Asticcacaulis biprosthecum. Arch Microbiol **118**:157–168.

661 27. **Ong CJ**, **Wong ML**, **Smit J**. 1990. Attachment of the adhesive holdfast organelle to the
662 cellular stalk of *Caulobacter crescentus*. J Bacteriol **172**:1448–1456.

663 28. **van Opijnen T**, **Bodi KL**, **Camilli A**. 2009. Tn-seq: high-throughput parallel sequencing for
664 fitness and genetic interaction studies in microorganisms. Nature Methods **6**:767–772.

665 29. **Wetmore KM**, **Price MN**, **Waters RJ**, **Lamson JS**, **He J**, **Hoover CA**, **Blow MJ**, **Bristow J**,
666 **Butland G**, **Arkin AP**, **Deutschbauer A**. 2015. Rapid Quantification of Mutant Fitness in
667 Diverse Bacteria by Sequencing Randomly Bar-Coded Transposons. mBio **6**:e00306–15–15.

668 30. **Awram P**, **Smit J**. 2001. Identification of lipopolysaccharide O antigen synthesis genes
669 required for attachment of the S-layer of Caulobacter crescentus. Microbiology **147**:1451–
670 1460.

671 31. **Jiang XM**, **Neal B**, **Santiago F**, **Lee SJ**, **Romana LK**, **Reeves PR**. 1991. Structure and
672 sequence of the rfb (O antigen) gene cluster of Salmonella serovar typhimurium (strain
673 LT2). Mol Microbiol **5**:695–713.

674 32. **Hardy GG**, **Toh E**, **Berne C**, **Brun YV**. 2018. Mutations in Sugar-Nucleotide Synthesis Genes
675 Restore Holdfast Polysaccharide Anchoring to Caulobacter crescentus Holdfast Anchor
676 Mutants. J Bacteriol **200**:e00597–17–24.

677 33. **Walker SG**, **Karunaratne DN**, **Ravenscroft N**, **Smit J**. 1994. Characterization of mutants of
678 Caulobacter crescentus defective in surface attachment of the paracrystalline surface layer. J
679 Bacteriol **176**:6312–6323.

680 34. **Dingwall A**, **Gober JW**, **Shapiro L**. 1990. Identification of a Caulobacter basal body
681 structural gene and a cis-acting site required for activation of transcription. J Bacteriol
682 **172**:6066–6076.

683 35. **Christen M**, **Beusch C**, **Bösch Y**, **Cerletti D**, **Flores-Tinoco CE**, **Del Medico L**, **Tschan F**,
684 **Christen B**. 2016. Quantitative Selection Analysis of Bacteriophage φCbK Susceptibility in
685 Caulobacter crescentus. J Mol Biol **428**:419–430.

686 36. **Haiko J**, **Westerlund-Wikström B**. 2013. The Role of the Bacterial Flagellum in Adhesion
687 and Virulence. Biology **2**:1242–1267.

688 37. **Wang Y**, **Haitjema CH**, **Fuqua C**. 2014. The Ctp type IVb pilus locus of Agrobacterium
689 tumefaciens directs formation of the common pili and contributes to reversible surface
690 attachment. J Bacteriol, 2nd ed. **196**:2979–2988.

691 38. **Aldridge P**, **Paul R**, **Goymer P**, **Rainey P**, **Jenal U**. 2003. Role of the GGDEF regulator PleD
692 in polar development of Caulobacter crescentus. Mol Microbiol **47**:1695–1708.

693 39. **Levi A**, **Jenal U**. 2006. Holdfast Formation in Motile Swarmer Cells Optimizes Surface
694 Attachment during Caulobacter crescentus Development. J Bacteriol **188**:5315–5318.

695 40. **Berne C**, **Ellison CK**, **Agarwal R**, **Severin GB**, **Fiebig A**, **Morton RI III**, **Waters CM**, **Brun**
696 **YV**. 2018. Feedback regulation of Caulobacter crescentusholdfast synthesis by flagellum
697 assembly via the holdfast inhibitor HfiA. Mol Microbiol **9**:e1003744–20.

698 41. **Price MN**, **Wetmore KM**, **Waters RJ**, **Callaghan M**, **Ray J**, **Liu H**, **Kuehl JV**, **Melnyk RA**,
699 **Lamson JS**, **Suh Y**, **Carlson HK**, **Esquivel Z**, **Sadeeshkumar H**, **Chakraborty R**, **Zane GM**,
700 **Rubin BE**, **Wall JD**, **Visel A**, **Bristow J**, **Blow MJ**, **Arkin AP**, **Deutschbauer AM**. 2018.
701 Mutant phenotypes for thousands of bacterial genes of unknown function. Nature **557**:503–
702 509.

703 42. **Hoffman MD**, **Zucker LI**, **Brown PJB**, **Kysela DT**, **Brun YV**, **Jacobson SC**. 2015. Timescales
704 and Frequencies of Reversible and Irreversible Adhesion Events of Single Bacterial Cells.
705 Anal Chem **87**:12032–12039.

706 43. **Nesper J**, **Hug I**, **Kato S**, **Hee C-S**, **Habazettl JM**, **Manfredi P**, **Grzesiek S**, **Schirmer T**,
707 **Emonet T**, **Jenal U**. 2017. Cyclic di-GMP differentially tunes a bacterial flagellar motor
708 through a novel class of CheY-like regulators. eLife **6**:1–25.

709 44. **Leclerc G**, **Wang SP**, **Ely B**. 1998. A new class of Caulobacter crescentus flagellar genes. J
710 Bacteriol **180**:5010–5019.

711 45. **O'Riordan K**, **Lee JC**. 2004. *Staphylococcus aureus* Capsular Polysaccharides. Clin Microbiol
712 Rev **17**:218–234.

713 46. **Stenutz R**, **Weintraub A**, **Widmalm G**. 2006. The structures of *Escherichia coli* O-
714 polysaccharide antigens. FEMS Microbiology Reviews **30**:382–403.

715 47. **Olivier NB**, **Chen MM**, **Behr JR**, **Imperiali B**. 2006. In Vitro Biosynthesis of UDP- N, N'-
716 Diacetylbacillosamine by Enzymes of the Campylobacter jejuniGeneral Protein
717 Glycosylation System †. Biochemistry **45**:13659–13669.

718 48. **Mostafavi AZ**, **Troutman JM**. 2013. Biosynthetic Assembly of the Bacteroides
719 fragilisCapsular Polysaccharide A Precursor Bactoprenyl Diphosphate-Linked Acetamido-4-
720 amino-6-deoxygalactopyranose. Biochemistry **52**:1939–1949.

721 49. **Ely B**. 1991. Genetics of Caulobacter crescentus. Meth Enzymol **204**:372–384.

722 50. **Thanbichler M**, **Iniesta AA**, **Shapiro L**. 2007. A comprehensive set of plasmids for
723 vanillate- and xylose-inducible gene expression in Caulobacter crescentus. Nucleic Acids
724 Research **35**:e137–e137.

725 51. **Hentchel KL**, **Ruiz LMR**, **Curtis PD**, **Fiebig A**, **Coleman ML**, **Crosson S**. 2018. Genome-scale
726 fitness profile of Caulobacter crescentus grown in natural freshwater. The ISME Journal 1–
727 14.

728 52. **Eisen MB**, **Spellman PT**, **Brown PO**, **Botstein D**. 1998. Cluster analysis and display of
729 genome-wide expression patterns. Proc Natl Acad Sci U S A **95**:14863–14868.

730 53. **Walker SG**, **Smith SH**, **Smit J**. 1992. Isolation and comparison of the paracrystalline surface
731 layer proteins of freshwater caulobacters. J Bacteriol **174**:1783–1792.

732 54. **Darveau RP**, **Hancock RE**. 1983. Procedure for isolation of bacterial lipopolysaccharides
733 from both smooth and rough Pseudomonas aeruginosa and Salmonella typhimurium
734 strains. J Bacteriol **155**:831–838.

735 55. **Kittelberger R**, **Hilbink F**. 1993. Sensitive silver-staining detection of bacterial
736 lipopolysaccharides in polyacrylamide gels. J Biochem Biophys Methods **26**:81–86.

737

738

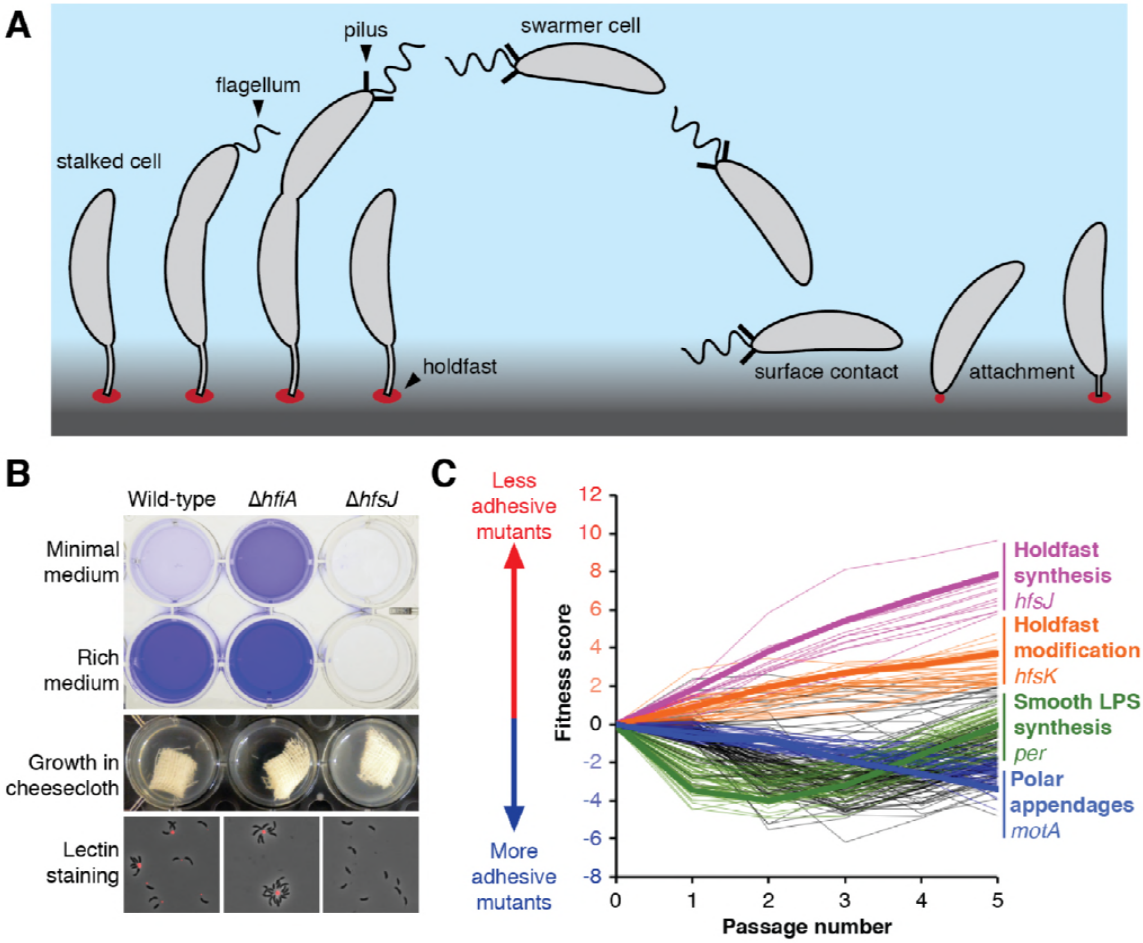

Figure 1 *A genome-wide screen for holdfast biosynthesis genes identifies multiple classes of mutants affecting adhesion*

A) During the dimorphic *C. crescentus* life-cycle, each cell division produces a motile swarmer cell and a sessile stalked cell. Swarmer cells stop swimming, shed their flagellum and pili and develop into stalked cells before dividing. Stalked cells adhere strongly to exogenous surfaces using a specialized material called the holdfast. B) The holdfast can be visualized by staining with fluorescently labeled wheat germ agglutinin (fWGA) and biofilm formation can be quantified by crystal violet staining. Δ*hfiA* cells overproduce holdfast and are hyper-adhesive. Δ*hfsJ* cells do not produce holdfasts and are non-adhesive. Attachment is reduced in minimal medium due to high levels of *hfiA* expression. C) Fitness profiles for the 250 genes with the strongest adhesion phenotypes in the cheesecloth passaging experiment. Lines are drawn to connect mean fitness scores at days zero through five for each of the 250 genes. Genes in the four major fitness clusters are colored according to the legend, with a specific example listed. Genes shown in black do not fit into the any of the four clusters.

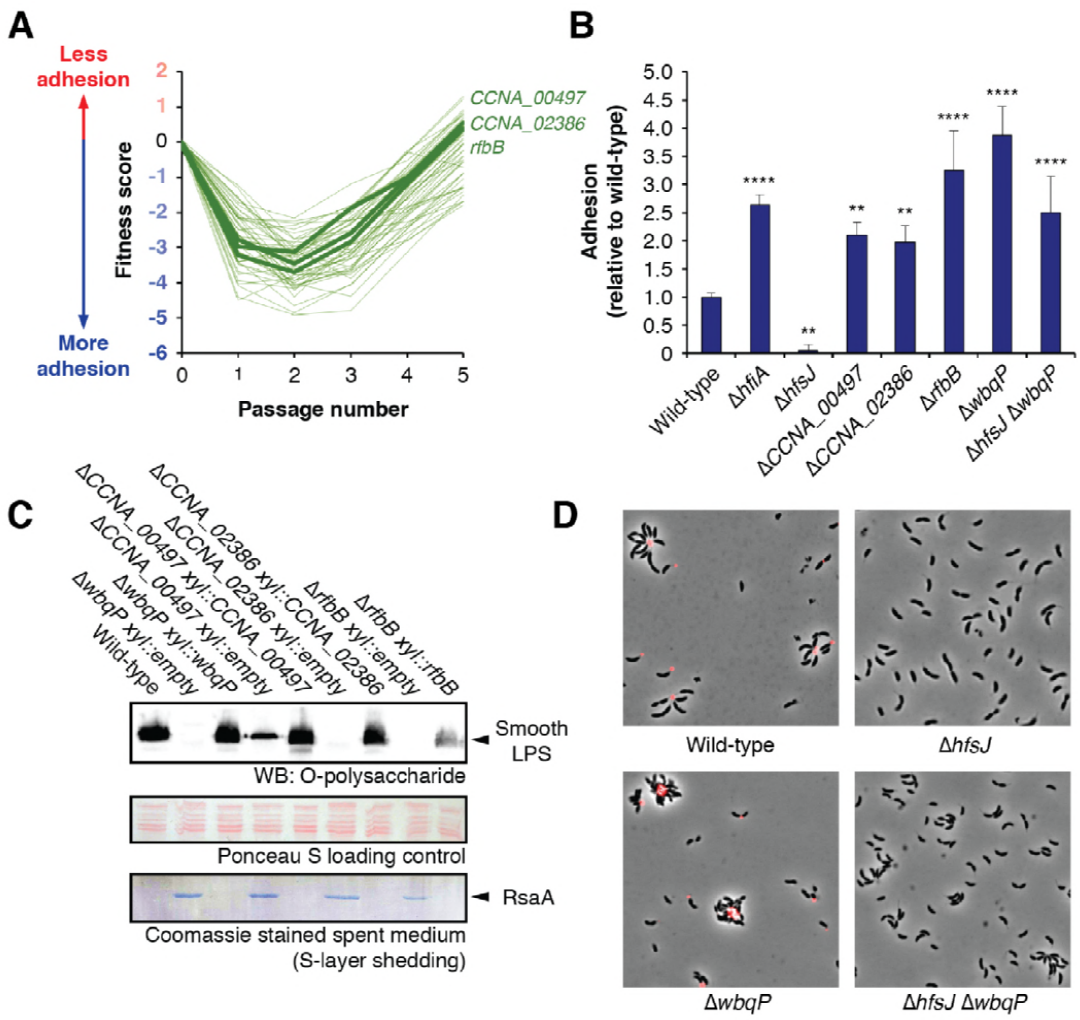

Figure 2 *Disrupting SLPS production leads to ectopic adhesion*
A) Fitness profiles for genes in the SLPS cluster. A full list of these genes and their annotations is provided in Table S3. *wbqP* was not characterized in our library due to low insertion density in this region. B) Surface attachment of SLPS mutants measured by CV staining. Cultures were grown for 24 hours in M2X medium before staining surface attached cells. Disrupting SLPS leads to increased adhesion in a holdfast-independent fashion. The graph shows the average (± standard deviation) of five biological replicates. Statistical significance was assessed by ANOVA with a pairwise Dunnett's post test to determine which samples differed from wild type. ns – not significant; * $P < 0.05$; ** $P < 0.01$; *** $P < 0.001$; **** $P < 0.0001$. C) Smooth LPS production is disrupted in Δ*CC_0465,* Δ*CC_2301* and Δ*rfbB*. Top: western blot to detect SLPS. Middle: Total protein stained with ponceau S as a loading control for SLPS blot. Bottom: Coomassie staining of spent medium from the cultures. Each mutant shows a loss of or a decrease in SLPS production by western blot and releases the S-layer protein RsaA into the spent medium. The cell-surface defects can be complemented by ectopic expression of the appropriate gene. "Empty" refers to plasmid control strains without inserts. D) fWGA staining (shown in red) shows ectopic adhesion in the Δ*wbqP* mutant. The rosettes in Δ*wbqP* cells are more compact than wild-type and have a different shape. Δ*hfsJ* Δ*wbqP* cells aggregate despite the lack of holdfasts and this aggregation occurs throughout the cell surface.

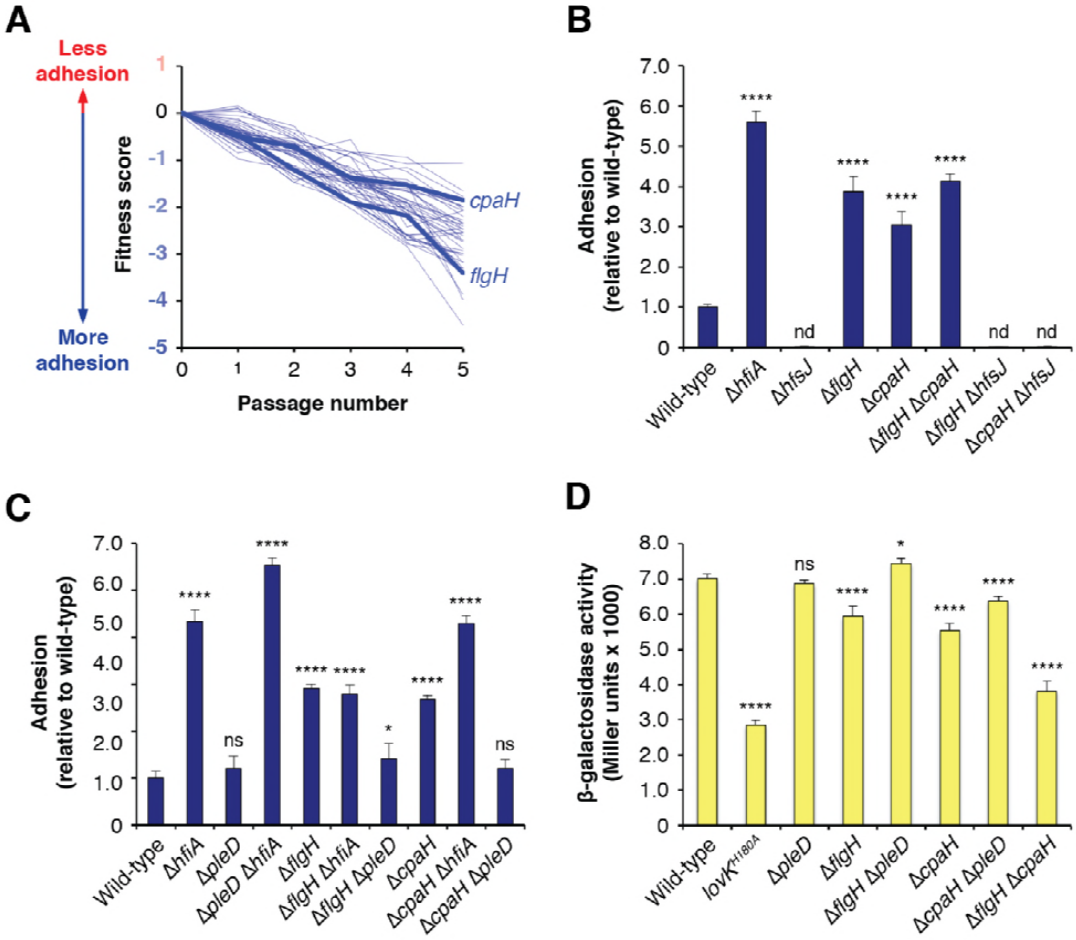

Figure 3 *Disrupting polar appendages stimulates holdfast production*
A) Fitness profiles for genes in the polar appendage cluster. A full list of these genes and their annotations is provided in Table S3. B) Surface attachment of motility mutants measured by CV staining. Cultures were grown for 17 hours in M2X medium before staining surface attached cells. Deletion of the genes for either the outer-membrane flagellar base protein FlgH or the inner-membrane type IV pilus component CpaH caused increased adhesion. In both mutant backgrounds, *hfsJ* is required for attachment. The graph shows the average (± standard deviation) of five biological replicates. C) Effect of *hfiA* and *pleD* deletions on surface attachment of *cpaH* and *flgH* mutants. Δ*hfiA* does not affect adhesion in the Δ*flgH* background and increases adhesion in the Δ*cpaH* background. The increased adhesion in both the Δ*flgH* and Δ*cpaH* mutants can be eliminated by deletion of *pleD.* The graph shows the average (± standard deviation) of four biological replicates. D) P_{hfiA}-*lacZ* reporter activity in motility mutants. The chart shows the average (± standard deviation) of four biological replicates. Statistical significance was assessed by ANOVA with a pairwise Dunnett's post test to determine which samples differed from wild type. nd – not detected; ns – not significant; * $P < 0.05$; ** $P < 0.01$; *** $P < 0.001$; **** $P < 0.0001$. When necessary, P values for additional pairwise comparisons pertinent to interpretation are indicated in the text.

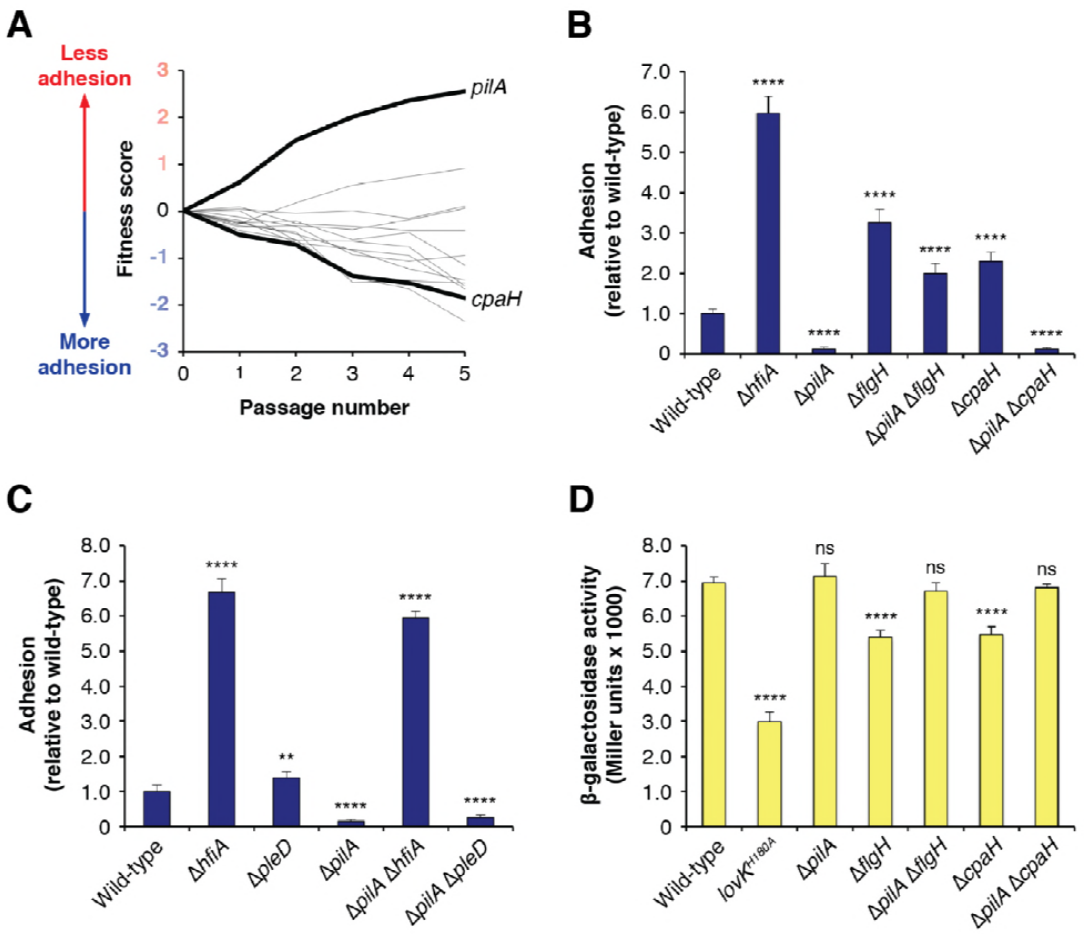

Figure 4 *Opposing effects of pilus mutants on adhesion*
A) Fitness profiles for genes at the pilus assembly locus. A full list of these genes and their annotations is provided in Table S3. B) Surface attachment of pilus mutants measured by CV staining. Cultures were grown for 17 hours in M2X medium before staining. Deletion of the gene for the main pilin subunit (PilA) reduces adhesion. Δ*pilA* is epistatic to Δ*cpaH* but not Δ*flgH.* The graph shows the average (± standard deviation) of seven biological replicates. C) Effect of *hfiA* and *pleD* deletions surface attachment in the Δ*pilA* background. Staining is slightly lower in Δ*hfiA* Δ*pilA* than Δ*hfiA* reflecting the holdfast-independent defect in surface attachment when the pilus is disrupted. *pleD* has no effect on adhesion in the Δ*pilA* mutant. The graph shows the average (± standard deviation) of six biological replicates. D) P_{hfiA}-*lacZ* reporter activity in various *pilA* mutants. The chart shows the average (± standard deviation) of four biological replicates. Statistical significance was assessed by ANOVA with a pairwise Dunnett's post test to determine which samples differed from wild type. ns – not significant; * $P < 0.05$; ** $P < 0.01$; *** $P < 0.001$; **** $P < 0.0001$. When necessary, P values for additional pairwise comparisons pertinent to interpretation are indicated in the text.

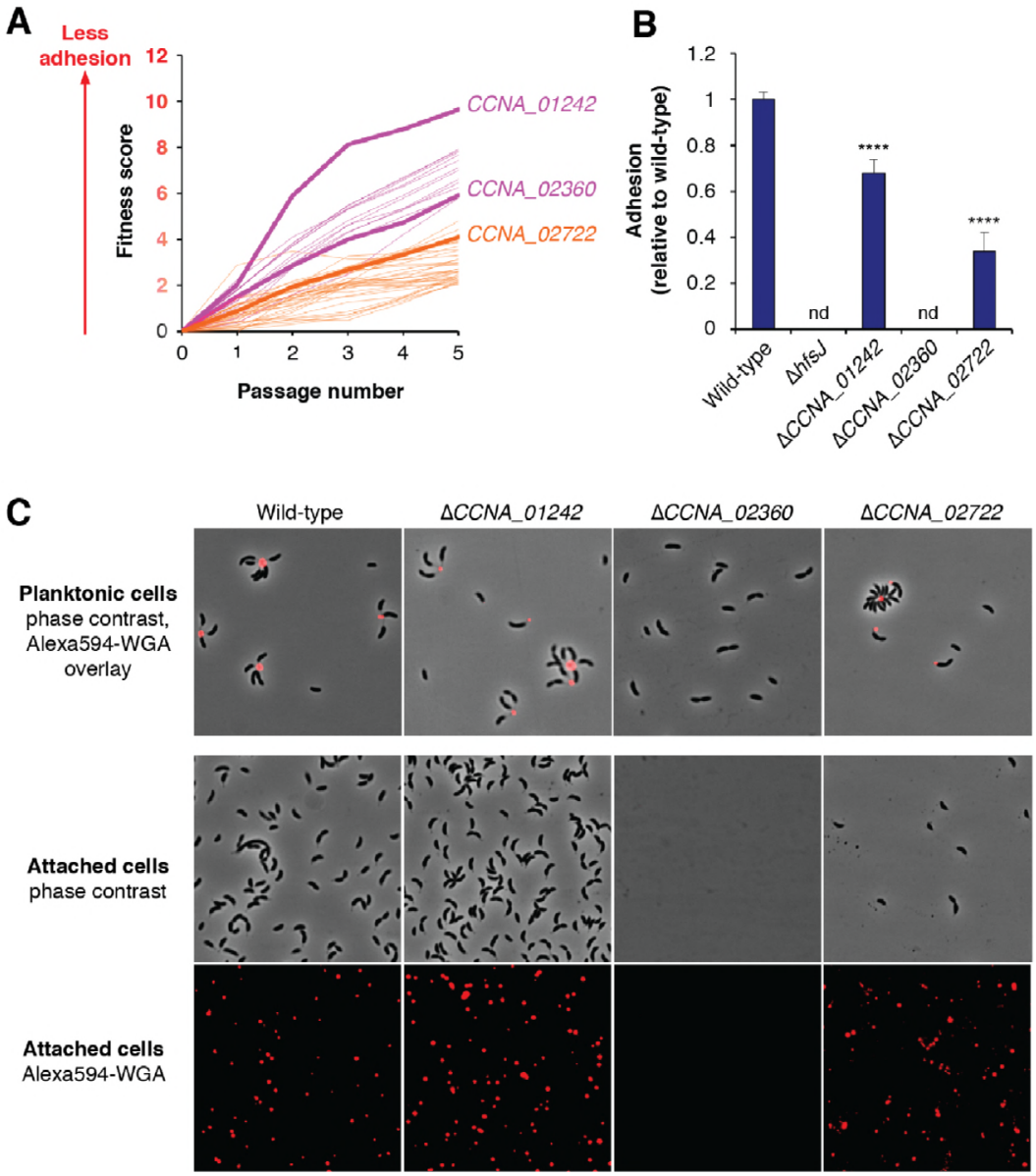

Figure 5 *New holdfast biosynthesis factors*
A) Fitness profiles for genes in the *hfs* (magenta) and holdfast modification (orange) clusters. Full lists of these genes and their annotations are provided in Table S3. B) Surface attachment of putative holdfast mutants measured by CV staining. Cultures were grown for 24 hours in PYE medium before being stained. Δ*CCNA_01242* and Δ*CCNA_02722* displayed reduced staining, and Δ*CCNA_02360* was non-adhesive. The graph shows the average (± standard deviation) of five biological replicates. C) Analysis of holdfast phenotypes by fWGA staining. The top panels show overlays of phase contrast and fluorescence images after staining planktonic cells as described in materials and methods. Adherent cells from the slide attachment assay are shown as phase contrast images in the middle set of panel, and the fluorescence channel showing attached holdfast material from the same slides is represented in the bottom panels. Δ*CCNA_01242* does not have an apparent holdfast defect, Δ*CCNA_02722* has a holdfast attachment defect and Δ*CCNA_02360* does not produce holdfasts. Statistical significance was assessed by ANOVA with a pairwise Dunnett's

833 post test to determine which samples differed from wild type. nd – not detected; ns – not
834 significant; * $P < 0.05$; ** $P < 0.01$; *** $P < 0.001$; **** $P < 0.0001$.
835

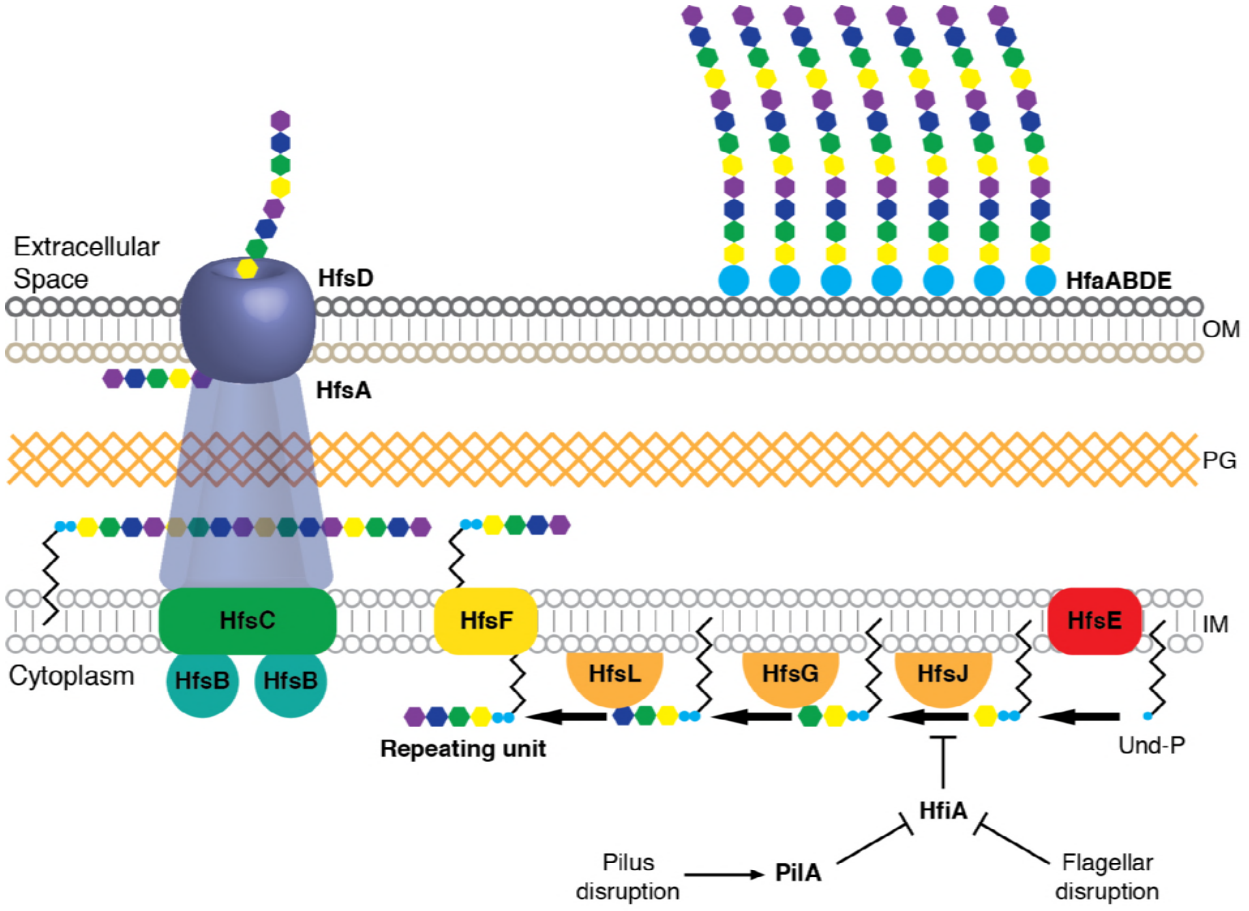

Figure 6 *Updated model for holdfast biosynthesis*
The model shows a *wzy*-type polysaccharide biosynthesis pathway. Four glycosyltransferases, HfsE, HfsJ, HfsG, and the newly described HfsL add monsaccharides sequentially onto the UP carrier to produce a glycolipid repeating unit. This intermediate is flipped across the membrane by HfsF, polymerized by HfsC and exported by a putative HfsABD transevelope complex. Attachment of the holdfast matrix is mediated by the Hfa proteins, including the newly-identified HfaE, reported here. Disruptions to the flagellum or the pilus activate holdfast production by relieving the inhibition of HfsJ by HfiA.

847 **Supplemental Materials**
848
849 **A genome-wide analysis of adhesion in *Caulobacter crescentus* identifies new**
850 **regulatory and biosynthetic components for holdfast assembly**
851
852 David M. Hershey, Aretha Fiebig and Sean Crosson
853

Strains				
Strain name	**Organism**	**Genotype**	**Description**	**Source**
FC19	*C. crescentus* CB15	CB15	Wild-type	ATCC 19089
FC1365	*C. crescentus* CB15	Δ*hfiA*	In-frame deletion of *CC_0817*	Ref. 10
FC1974	*C. crescentus* CB15	Δ*hfsJ*	In-frame deletion of *CC_0095*	Ref. 10
FC3105	*C. crescentus* CB15	Δ*pleD*	In-frame deletion of *CC_2462*	This work
FC3054	*C. crescentus* CB15	Δ*CCNA_00497*	In-frame deletion of *CC_0465*	This work
FC3055	*C. crescentus* CB15	Δ*CCNA_02386*	In-frame deletion of *CC_2301*	This work
FC3056	*C. crescentus* CB15	Δ*rfbB*	In-frame deletion of *CC_3629*	This work
FC3057	*C. crescentus* CB15	Δ*wbqP*	In-frame deletion of *CC_1486*	This work
FC3058	*C. crescentus* CB15	Δ*hfsJ* Δ*wbqP*	In-frame deletion of *CC_1486* in FC1974 background	This work
FC1266	*C. crescentus* CB15	Δ*flgH*	In-frame deletion of *CC_2066*	This work
FC3013	*C. crescentus* CB15	Δ*cpaH*	In-frame deletion of *CC_2940*	This work
FC1265	*C. crescentus* CB15	Δ*pilA*	In-frame deletion of *CC_2948*	This work
FC3019	*C. crescentus* CB15	Δ*CCNA_01242*	In-frame deletion of *CC_1184*	This work
FC3021	*C. crescentus* CB15	Δ*hfsL*	In-frame deletion of *CC_2277*	This work
FC3020	*C. crescentus* CB15	Δ*hfaE*	In-frame deletion of *CC_2639*	This work
FC3015	*C. crescentus* CB15	Δ*hfsJ* Δ*flgH*	In-frame deletion of *CC_2066* in FC1974 background	This work
FC3016	*C. crescentus* CB15	Δ*hfsJ* Δ*cpaH*	In-frame deletion of *CC_2940* in FC1974 background	This work
FC3107	*C. crescentus* CB15	Δ*flgH* Δ*cpaH*	In-frame deletion of *CC_2940* in FC1266	This work
FC3085	*C. crescentus* CB15	Δ*flgH* Δ*hfiA*	In-frame deletion of *CC_0817* in FC1266 background	This work
FC3083	*C. crescentus* CB15	Δ*cpaH* Δ*hfiA*	In-frame deletion of *CC_0817* in FC3013 background	This work
FC3084	*C. crescentus* CB15	Δ*pilA* Δ*hfiA*	In-frame deletion of *CC_0817* in FC1265 background	This work
FC3104	*C. crescentus* CB15	Δ*flgH* Δ*pleD*	In-frame deletion of *CC_2462* in FC1266 background	This work
FC3103	*C. crescentus* CB15	Δ*cpaH* Δ*pleD*	In-frame deletion of *CC_2462* in FC3013 background	This work
FC3108	*C. crescentus* CB15	Δ*pilA* Δ*pleD*	In-frame deletion of *CC_2462* in FC1265 background	This work
FC3017	*C. crescentus* CB15	Δ*flgH* Δ*pilA*	In-frame deletion of *CC_2948* in FC1266 background	This work

FC3018	*C. crescentus* CB15	Δ*cpaH* Δ*pilA*	In-frame deletion of *CC_2948* in FC3013 background	This work
FC3097	*C. crescentus* CB15	Δ*CCNA_00497 xyl::P$_{xyl}$-empty*	pMT585 integrated at xylose locus of FC3054	This work
FC3098	*C. crescentus* CB15	Δ*CCNA_00497 xyl::P$_{xyl}$-CCNA_00497*	pFC3080 integrated at xylose locus of FC3054	This work
FC3101	*C. crescentus* CB15	Δ*CCNA_02386 xyl::P$_{xyl}$-empty*	pMT585 integrated at xylose locus of FC3055	This work
FC3102	*C. crescentus* CB15	Δ*CCNA_02386 xyl::P$_{xyl}$-CCNA_02386*	pFC3082 integrated at xylose locus of FC3055	This work
FC3095	*C. crescentus* CB15	Δ*rfbB xyl::P$_{xyl}$-empty*	pMT585 integrated at xylose locus of FC3056	This work
FC3096	*C. crescentus* CB15	Δ*rfbB xyl::P$_{xyl}$-rfbB*	pFC3079 integrated at xylose locus of FC3056	This work
FC3099	*C. crescentus* CB15	Δ*wbqP xyl::P$_{xyl}$-empty*	pMT585 integrated at xylose locus of FC3057	This work
FC3100	*C. crescentus* CB15	Δ*wbqP xyl::P$_{xyl}$-wbqP*	pFC3081 integrated at xylose locus of FC3057	This work
FC3075	*C. crescentus* CB15	Δ*flgH xyl::P$_{flgE}$-empty*	pFC3094 integrated at xylose locus of FC1266	This work
FC3074	*C. crescentus* CB15	Δ*flgH xyl::P$_{flgE}$-flgH*	pFC3093 integrated at xylose locus of FC1266	This work
FC3070	*C. crescentus* CB15	Δ*cpaH xyl::P$_{xyl}$-empty*	pMT585 integrated at xylose locus of FC3013	This work
FC3071	*C. crescentus* CB15	Δ*cpaH xyl::P$_{xyl}$-cpaH*	pFC3090 integrated at xylose locus of FC3013	This work
FC3073	*C. crescentus* CB15	Δ*pilA xyl::P$_{pilA}$-empty*	pFC3092 integrated at xylose locus of FC1265	This work
FC3072	*C. crescentus* CB15	Δ*pilA xyl::P$_{pilA}$-pilA*	pFC3091 integrated at xylose locus of FC1265	This work
FC3126	*C. crescentus* CB15	Δ*CCNA_01242 xyl::P$_{CCNA_01242}$-empty*	pFC3124 integrated at xylose locus of FC3019	This work
FC3127	*C. crescentus* CB15	Δ*CCNA_01242 xyl::P$_{CCNA_01242}$-CCNA_01242*	pFC3125 integrated at xylose locus of FC3019	This work
FC3088	*C. crescentus* CB15	Δ*hfsL xyl::P$_{xyl}$-empty*	pMT585 integrated at xylose locus of FC3021	This work
FC3089	*C. crescentus* CB15	Δ*hfsL xyl::P$_{xyl}$-hfsL*	pFC3078 integrated at xylose locus of FC3021	This work
FC3086	*C. crescentus* CB15	Δ*hfaE xyl::P$_{xyl}$-empty*	pMT585 integrated at xylose locus of FC3020	This work
FC3087	*C. crescentus* CB15	Δ*hfaE xyl::P$_{xyl}$-*	pFC3077 integrated at xylose	This work

		hfaE	locus of FC3020	
APA_752	*E. coli* WM3064	Tn-HiMar (Km^R)	Bacroded transposon pool for created BarSeq libraries	Ref. 29

Plasmids			
Plasmid name	**Description**	**Antibiotic**	**Reference**
pNPTS138	Suicide plasmid for making unmarked deletions in *C. crescentus*; carries sacB for counter-selection	Km	M. R Alley unpublished
pFC3059	To delete *CCNA_01242*; contains fusion of *CC_1184* flanking regions with first and last 12 nucleotides of *CC_1184* ORF included	Km	This work
pFC3060	To delete *hfaE*; contains fusion of *CC_2639* flanking regions with first and last 12 nucleotides of *CC_2639* ORF included	Km	This work
pFC3061	To delete *hfsL*; contains fusion of *CC_2277* flanking regions with first 12 and last 96 nucleotides of *CC_2277* ORF included	Km	This work
pFC3063	To delete *CCNA_00497*; contains fusion of *CC_0465* flanking regions with first and last 12 nucleotides of *CC_0465* ORF included	Km	This work
pFC3062	To delete *CCNA_02386*; contains fusion of *CC_2301* flanking regions with first and last 12 nucleotides of *CC_2301* ORF included	Km	This work
pFC3068	To delete *rfbB*; contains fusion of *CC_3629* flanking regions with first and last 12 nucleotides of *CC_3629* ORF included	Km	This work
pFC3069	To delete *wbqP*; contains fusion of *CC_1486* flanking regions with first and last 12 nucleotides of *CC_1486* ORF included	Km	This work
pFC1267	To delete *pilA*; contains fusion of *CC_2948* flanking regions with first and last 12 nucleotides of *CC_2948* ORF included	Km	This work
pFC1268	To delete *flgH*; contains fusion of *CC_2066* flanking regions with first and last 12 nucleotides of *CC_2066* ORF included	Km	This work
pFC3065	To delete *cpaH*; contains fusion of *CC_2940* flanking regions with first and last 12 nucleotides of *CC_2940* ORF included	Km	This work
pFC3067	To delete *pleD*; contains fusion of *CC_2462* flanking regions with first and last 12 nucleotides of*CC_2462* ORF included	Km	This work
pMT585	Contains multiple cloning site downstream of Pxyl; integrates at upstream of *xylX*; used for complementations	Km	Ref. 50
pFC3077	pMT585 containing *hfaE* under the control of P_{xyl} for	Km	This work

	integration at *xylX* locus		
pFC3078	pMT585 containing *hfsL* under the control of P_{xyl} for integration at *xylX* locus	Km	This work
pFC3080	pMT585 containing *CCNA_00497* under the control of P_{xyl} for integration at *xylX* locus	Km	This work
pFC3082	pMT585 containing *CCNA_02386* under the control of P_{xyl} for integration at *xylX* locus	Km	This work
pFC3079	pMT585 containing *rfbB* under the control of P_{xyl} for integration at *xylX* locus	Km	This work
pFC3081	pMT585 containing *wbqP* under the control of P_{xyl} for integration at *xylX* locus	Km	This work
pFC3091	pMT585 containing *pilA* under the control of P_{pilA} for integration at *xylX* locus; 316bp upstream of *CC_2948* fused to the *CC_2948* ORF was inserted in reverse oreintation into pMT585	Km	This work
pFC3092	pMT585 containing P_{pilA} without insert for integration at *xylX* locus; 316bp upstream of *CC_2948* was inserted in reverse orientation into pMT585	Km	This work
pFC3093	pMT585 containing *flgH* under the control of P_{flgF} for integration at *xylX* locus; 226bp upstream of *CC_2063* fused to the *CC_2066* ORF was inserted in reverse oreintation into pMT585	Km	This work
pFC3094	pMT585 containing P_{flgE} without insert for integration at *xylX* locus; 216bp upstream of *CC_2063* was inserted in reverse orientation into pMT585	Km	This work
pFC3090	pMT585 containing *cpaH* under the control of P_{xyl} for integration at *xylX* locus	Km	This work
pFC3124	pMT585 containing P_{CCNA_01242} without insert for integration at *xylX* locus; 99bp upstream of the *CC_1184* ORF was inserted in reverse orientation into pMT585	Km	This work
pFC3124	pMT585 containing *CCNA_01242* under the control of P_{CCNA_01242} for integration at *xylX* locus; 99bp upstream of *CC_1184* fused to the *CC_1184* ORF was inserted in reverse oreintation into pMT585	Km	This work
pFC1948	pRKlac290 containing the *hfiA* promoter fused to *lacZ*	Tet	Ref. 10

854
855 **Table S1** *Strains and plasmids used in this study*
856 To analyze the sequence data used for fitness calculations, we used the *C. crescentus* NA1000
857 genome. NA1000 is directly derived from CB15, but its genome has more detailed annotations and
858 is better curated. To facilitate interpretation of the BarSeq data, genotypes in the text and
859 supplemental tables use the NA1000 locus numbers and nomenclature. We note the
860 corresponding CB15 numbers in the "Description" column.
861

Sample name	Index	Sample description	Total reads	Usable reads	Unique barcodes	Proportion of reads in top percentile
SCD_50.31	CACGAT	PYE 1A	4018890	3698106	233280	0.117
SCD_50.32	CACTCA	PYE 1B	4492543	4130359	246118	0.1227
SCD_50.33	CAGGCG	PYE 1C	4449306	4044087	150780	0.1236
SCD_50.34	CATGGC	PYE 2A	4137845	3779486	226993	0.1249
SCD_50.35	CATTTT	PYE 2B	4499135	4137664	228359	0.1274
SCD_50.36	CCAACA	PYE 2C	4213003	3750243	228855	0.1316
SCD_50.37	CGGAAT	PYE 3A	6735128	6171057	262618	0.1504
SCD_50.38	CTAGCT	PYE 3B	6127591	5614129	249692	0.1471
SCD_50.39	CTATAC	PYE 3C	5796738	5301288	246006	0.1563
SCD_50.40	CTCAGA	PYE 4A	5322215	4857843	235579	0.1571
SCD_50.41	GACGAC	PYE 4B	6394697	5855783	248801	0.1691
SCD_50.42	TAATCG	PYE 4C	2975382	2755150	172812	0.1675
SCD_50.43	TACAGC	PYE 5A	5799597	5301223	246151	0.2002
SCD_50.44	TATAAT	PYE 5B	6016430	5569218	234947	0.1972
SCD_50.45	TCATTC	PYE 5C	4811202	4428232	209890	0.2178
SCD_50.46	TCCCGA	Cheese 1A	4562846	4108435	242916	0.1455
SCD_50.47	TCGAAG	Cheese 1B	4313848	3922295	233599	0.1484
SCD_50.48	TCGGCA	Cheese 1C	4773752	4335186	247032	0.1516
SCD_50.49	AAACAT	Cheese 2A	6050903	5557666	232487	0.2488
SCD_50.50	AAAGCA	Cheese 2B	7013967	6384659	253431	0.2793
SCD_50.51	AAATGC	Cheese 2C	4421479	4054218	211068	0.2713
SCD_50.52	AACAAA	Cheese 3A	6616953	5904400	235379	0.4118
SCD_50.53	AACTTG	Cheese 3B	5935535	5450038	209707	0.4585
SCD_50.54	AAGACT	Cheese 3C	7750956	7158882	204209	0.5887
SCD_50.55	AAGCGA	Cheese 4A	4002747	3664336	167909	0.6349
SCD_50.56	AAGGAC	Cheese 4B	3156990	2902069	151371	0.605
SCD_50.57	AATAGG	Cheese 4C	1882499	1730719	115437	0.6777
SCD_50.58	ACAAAC	Cheese 5A	2475323	2197424	99108	0.787
SCD_50.59	ACATCT	Cheese 5B	2419554	2241238	99833	0.7796
SCD_5060	ACCCAG	Cheese 5C	2865211	2583906	107021	0.8014

Table S2 *Samples used for BarSeq analysis of gene fitness across cheesecloth passages*
The "Index" column represents the TruSeq indices used to de-multiplex the samples after sequencing. Cheese and PYE represent passages with and without cheesecloth, respectively. The numbers indicate which of the five passages each sample represents, and the letters indicate which of the three replicates. The "Proportion of reads in top percentile" column is calculated by ranking the barcodes in each sample by their abundance and determining the proportion of reads that map to the top 1% of barcodes.

Cluster 1: SLPS						
locusId; annotation	**0**	**1**	**2**	**3**	**4**	**5**
CCNA_00044; ribosome maturation protein RimP	0.013	-2.93	-4.145	-3.319	-1.57	-0.067
CCNA_00217; thiol:disulfide interchange protein DsbD	-0.07	-2.488	-2.869	-1.883	-0.313	1.215
CCNA_00290; autotransporter protein	0.009	-3.141	-3.74	-3.294	-2.788	-1.794
CCNA_00390; ADP-heptose--LPS heptosyltransferase	-0.008	-2.321	-4.402	-2.913	-2.413	-1.408
CCNA_00497; putative rhamnosyl transferase	-0.074	-3.219	-3.706	-2.835	-1.19	0.371
CCNA_00502; glycosyl transferase family protein	0.024	-3.405	-3.06	-3.883	-2.296	-1.313
CCNA_00512; GTP-binding protein, probable translation factor	0.082	-3.203	-3.936	-3.087	-1.455	0.104
CCNA_00519; conserved hypothetical protein	0.009	-4.406	-4.912	-4.798	-3.134	-1.521
CCNA_00667; lipopolysaccharide biosynthesis protein	-0.194	-2.497	-2.358	-1.846	-0.306	1.286
CCNA_00668; capsular polysaccharide biosynthesis protein	-0.001	-2.031	-3.171	-3.547	-1.836	-1.285
CCNA_00669; glycosyltransferase family 99 protein WbsX	-0.022	-3.396	-3.205	-2.343	-0.788	0.792
CCNA_01055; GT1 family glyscosyl transferase	-0.043	-3.088	-4.106	-3.578	-2.06	-0.533
CCNA_01062; GDP-mannose 4,6 dehydratase	-0.117	-3.685	-4.072	-3.613	-1.995	-0.595
CCNA_01063; UDP-perosamine 4-acetyl transferase	-0.038	-3.41	-2.969	-2.665	-0.986	0.2
CCNA_01064; perosamine synthetase	-0.112	-3.481	-4	-3.214	-1.594	-0.064
CCNA_01065; glycosyltransferase	-0.076	-3.761	-3.547	-3.178	-1.581	-0.043
CCNA_01066; glycosyltransferase	-0.038	-2.802	-3.277	-2.57	-1.632	-0.394
CCNA_01068; glycosyltransferase	-0.15	-4.496	-3.787	-3.662	-1.324	-0.508
CCNA_01086; GTP-binding protein lepA	0.043	-3.449	-3.931	-3.509	-2.112	-0.57
CCNA_01103; ADP-heptose--LPS heptosyltransferase	0.034	-2.691	-2.823	-3.069	-1.778	-0.077
CCNA_01199; glucose-1-phosphate thymidylyltransferase	-0.008	-4.037	-3.851	-3.099	-1.424	0.062
CCNA_01375; lactoylglutathione lyase	0.048	-3.392	-4.654	-4.066	-	-

					2.463	1.058
CCNA_01427; beta-barrel assembly machine (BAM) protein BamE	0.052	-2.633	-4.028	-4.39	-2.727	-1.235
CCNA_01430; conserved hypothetical protein	-0.013	-1.923	-2.959	-3.144	-2.08	-0.903
CCNA_01447; homoserine dehydrogenase	0.02	-2.348	-3.724	-2.91	-1.286	0.261
CCNA_01497; ADP-L-glycero-D-manno-heptose-6-epimerase	0.022	-2.19	-2.593	-2.199	-1.98	-0.42
CCNA_01955; zinc metalloprotease	0.005	-2.151	-2.316	-2.232	-1.865	-1.314
CCNA_01971; peptidyl-prolyl cis-trans isomerase	0.013	-2.17	-2.493	-1.791	-0.927	0.591
CCNA_02219; hypothetical protein	0.017	-2.85	-2.949	-2.521	-2.268	-1.687
CCNA_02326; acetylornithine aminotransferase/succinyldiaminopimelate aminotransferase	0.019	-1.712	-2.166	-1.194	-0.525	0.791
CCNA_02347; phosphomannomutase/phosphoglucomutase	-0.064	-4.09	-4.85	-4.033	-2.455	-0.889
CCNA_02386; O-antigen ligase related enzyme	-0.134	-2.762	-3.457	-2.585	-1.025	0.537
CCNA_02463; UDP-N-acetylglucosamine 4-epimerase	0.029	-2.627	-3.781	-3.758	-2.374	-0.882
CCNA_02650; N-acetyl-anhydromuramyl-L-alanine amidase	-0.018	-1.617	-3.035	-2.194	-0.678	0.911
CCNA_02941; transcription elongation factor greA	-0.119	-1.233	-2.748	-2.498	-0.92	0.629
CCNA_03026; two-component response regulator petR	-0.055	-2.619	-4.063	-3.652	-2.577	-1.705
CCNA_03195; RNA polymerase sigma factor RpoH	-0.001	-2.089	-3.735	-3.307	-1.951	-1.294
CCNA_03352; YebC/PmpR transcriptional regulator	-0.009	-3.942	-4.169	-3.705	-2.805	-1.706
CCNA_03475; homoserine kinase	-0.028	-1.569	-3.168	-2.323	-0.697	0.84
CCNA_03609; outer membrane protein	-0.011	-2.28	-3.936	-3.203	-1.489	-0.261
CCNA_03705; conserved hypothetical protein	0.053	-1.304	-3.383	-1.826	-0.864	0.665
CCNA_03713; RNA polymerase sigma-54 factor rpoN	0.02	-1.566	-3.418	-2.288	-1.299	0.198
CCNA_03733; mannose-1-phosphate guanylyltransferase	-0.137	-2.754	-3.111	-2.202	-1.085	0.29

CCNA_03744; dTDP-glucose 4,6-dehydratase	-0.009	-2.964	-3.124	-1.88	-1.002	0.388
CCNA_03748; dTDP-4-dehydrorhamnose 3,5-epimerase	-0.059	-2.155	-2.242	-1.967	-0.249	0.731
CCNA_03859; two-component response regulator cenR	0.01	-1.898	-3.244	-2.126	-0.879	0.579
CCNA_03909; conserved hypothetical protein	0.028	-2.113	-4.213	-2.917	-1.893	-0.234
CCNA_03984; hypothetical protein	0.007	-1.779	-2.747	-2.011	-0.292	-0.697
Cluster 2: Polar appendages						
locusId; annotation	**0**	**1**	**2**	**3**	**4**	**5**
CCNA_00233; UDP-N-acetylglucosamine 4,6-dehydratase	0.008	-0.398	-0.647	-1.464	-1.536	-1.994
CCNA_00234; WecE-family cell wall biogenesis enzyme	0.005	-0.587	-1.119	-1.518	-1.539	-2.71
CCNA_00444; chemotaxis protein methyltransferase	-0.017	-0.73	-1.261	-1.337	-1.85	-2.405
CCNA_00447; chemotaxis protein cheD	-0.008	-0.393	-1.262	-1.868	-2.689	-2.926
CCNA_00449; cheYIII	-0.001	-0.649	-1.243	-1.71	-2.675	-2.985
CCNA_00542; hypothetical protein	0.003	-0.471	-1.169	-1.452	-1.965	-2.529
CCNA_00787; chemotaxis motA protein	-0.012	-0.721	-0.806	-1.894	-2.588	-3.396
CCNA_00821; hypothetical protein	-0.027	-0.613	-1.472	-0.837	-1.245	-2.046
CCNA_00823; LuxR-like DNA-binding protein	-0.058	-0.97	-1.218	-1.518	-2.066	-2.612
CCNA_00942; flagellar hook-associated protein FlgL	0.004	-0.424	-0.765	-1.385	-1.835	-2.326
CCNA_00943; flagellar hook-associated protein FlaN	-0.032	0.105	-0.548	-0.928	-2.707	-2.553
CCNA_01004; flagellar basal-body rod protein FlgB	0.004	-0.37	-0.935	-1.357	-2.617	-3.031
CCNA_01005; flagellar basal-body rod protein flgC	0.004	-0.426	-0.738	-1.599	-2.121	-3.296
CCNA_01094; hypothetical protein	-0.002	0.146	-0.421	-1.277	-1.473	-3.97
CCNA_01117; conserved hypothetical protein	0.006	-0.472	-0.715	-1.256	-1.147	-1.777
CCNA_01524; FlbA protein	0.001	-0.427	-0.921	-1.919	-1.998	-2.886

CCNA_01527; flagellin fljL	0.011	-0.601	-1.477	-1.912	-2.791	-2.989
CCNA_01530; flagellin FljJ	-0.005	-0.245	-0.754	-1.332	-1.409	-2.203
CCNA_01532; regulatory protein flaY	0.004	-0.56	-0.887	-1.34	-1.497	-1.985
CCNA_01562; 4-hydroxy-2-oxoglutarate aldolase/2-dehydro-3-deoxyphosphogluconate aldolase	-0.001	0.111	-0.489	-1.482	-2.752	-3.307
CCNA_01644; chemotaxis motB protein	-0.002	-0.479	-0.629	-1.493	-2.599	-2.458
CCNA_01675; outer membrane protein	-0.008	-0.328	-0.695	-1.409	-1.926	-2.472
CCNA_01676; conserved hypothetical protein	0.006	-0.455	-0.55	-1.207	-2.14	-2.362
CCNA_02142; flagellar basal-body rod protein flgF	-0.011	-0.368	-1.402	-1.304	-2.054	-3.858
CCNA_02143; flagellar basal-body rod protein flgG	-0.008	-0.273	-1.237	-1.728	-2.163	-2.703
CCNA_02144; flagella basal body P ring formation protein flgA	0.004	-0.357	-0.887	-1.701	-1.911	-3.179
CCNA_02145; flagellar L-ring protein flgH	-0.005	-0.473	-1.193	-1.891	-2.175	-3.406
CCNA_02322; Co2+/Mg2+ efflux protein ApaG	0.01	-0.146	-0.529	-0.943	-1.572	-2.072
CCNA_02411; putative lytic transglycosylase PleA	0.008	-0.039	-0.349	-0.84	-1.079	-1.064
CCNA_02526; dihydroorotase	0	-0.85	-0.636	-1.913	-2.573	-3.177
CCNA_02667; flagellar basal-body protein FlbY	-0.011	-0.328	-0.781	-1.413	-1.898	-3.416
CCNA_02796; conserved hypothetical protein	-0.019	-0.623	-1.316	-2.031	-2.836	-4.51
CCNA_02946; spsF-related cytidylyltransferase	0.002	-0.342	-0.765	-1.462	-1.667	-1.885
CCNA_02947; spsG-related polysaccharide biosynthesis protein	0.007	-0.126	-0.843	-0.56	-2.42	-2.072
CCNA_02950; hypothetical protein	0.006	-0.564	-1.334	-1.874	-2.604	-2.534
CCNA_02951; WbqC-like family protein	0.011	-0.302	-0.744	-1.461	-1.905	-2.271
CCNA_02961; NeuB-family N-acetylneuraminate synthase	0.005	-0.404	-0.841	-1.145	-2.067	-2.738
CCNA_03035; TadC-related pilus assembly protein	0.013	-0.501	-0.716	-1.382	-1.531	-1.851

CCNA_03036; TadB-related pilus assembly protein	0.004	-0.411	-0.608	-1.411	-1.647	-2.348
CCNA_03041; pilus assembly protein CpaB	0.004	-0.193	-0.661	-0.824	-0.946	-1.653
CCNA_03890; conserved hypothetical protein	0.007	0.049	-0.268	-1.598	-1.602	-2.476
Cluster 3: Pilus assembly						
locusId; annotation	**0**	**1**	**2**	**3**	**4**	**5**
CCNA_03033; Flp pilus assembly protein TadD	0.008	0.009	-0.62	-0.629	-0.758	-1.594
CCNA_03035; TadC-related pilus assembly protein	0.013	-0.501	-0.716	-1.382	-1.531	-1.851
CCNA_03036; TadB-related pilus assembly protein	0.004	-0.411	-0.608	-1.411	-1.647	-2.348
CCNA_03037; pilus assembly ATPase CpaF	0.005	0.095	-0.253	-0.32	-0.409	-0.403
CCNA_03038; pilus assembly ATPase CpaE	-0.004	-0.237	-0.211	-0.606	-0.457	-1.147
CCNA_03039; pilus assembly protein CpaD	0.037	-0.125	-0.317	-0.922	-1.06	-0.943
CCNA_03040; outer membrane pilus secretion channel CpaC	0.008	-0.244	-0.478	-0.827	-1.23	-1.472
CCNA_03041; pilus assembly protein CpaB	0.004	-0.193	-0.661	-0.824	-0.946	-1.653
CCNA_03042; pilus assembly prepilin peptidase CpaA	-0.001	-0.267	0.188	0.554	0.736	0.911
CCNA_03043; type IV pilin protein pilA	0.006	0.615	1.513	2.023	2.366	2.569
CCNA_03044; CpaC-related secretion pathway protein	0.008	-0.301	-0.433	-1.517	-1.481	-1.527
CCNA_03045; TadG-related pilus assembly protein	0	0.045	-0.047	0.016	-0.154	0.109
CCNA_03046; TadE-related pilus assembly protein	-0.004	-0.33	-0.304	-0.389	-0.182	0.06
Cluster 4: Holdfast synthesis						
locusId; annotation	**0**	**1**	**2**	**3**	**4**	**5**
CCNA_00094; WecG/TagA-family glycosyltransferase HfsJ	-0.001	1.792	3.826	5.461	6.707	7.85
CCNA_01241; Zn-dependent hydrolase, glyoxalase II family	-0.014	0.565	2.753	4.296	5.334	6.595
CCNA_01242; amino acid permease	0.008	2.034	5.865	8.127	8.789	9.649
CCNA_02360; glycosyl transferase family 2 protein	0.006	1.507	2.857	3.987	4.727	5.919
CCNA_02436; hypothetical protein	-0.011	0.37	1.598	2.491	4.207	5.78

CCNA_02509; glycosyltransferase hfsG	0	1.44	2.961	4.334	5.264	6.452
CCNA_02510; oligosaccharide deacetylase hfsH	-0.002	1.328	3.155	4.619	5.782	6.993
CCNA_02512; polysaccharide autokinase-related protein hfsB	-0.005	1.819	3.721	5.31	6.57	7.798
CCNA_02513; holdfast synthesis protein HfsA	-0.002	1.823	3.702	5.359	6.375	7.653
CCNA_02514; polysaccharide secretin protein hfsD	0.001	1.8	3.812	5.491	6.638	7.911
CCNA_02567; sensory transduction histidine kinase pleC	0.002	2.23	4.093	5.298	6.293	7.414
CCNA_02711; holdfast attachment protein hfaA	-0.019	1.335	2.869	4.649	5.335	6.242
CCNA_02712; holdfast attachment protein hfaB	0.001	1.441	3.288	4.825	5.894	7.119
CCNA_02713; holdfast attachment protein hfaD	0.004	1.053	2.76	3.972	5.004	5.894
Cluster 5: Holdfast modification						
locusId; annotation	**0**	**1**	**2**	**3**	**4**	**5**
CCNA_00006; enoyl-CoA hydratase	0.006	1.416	2.106	2.633	2.838	2.885
CCNA_00011; chaperone protein DnaJ	-0.002	0.391	1.424	2.487	3.42	3.55
CCNA_00134; surface protein	0.012	1.004	1.223	2.175	2.703	3.104
CCNA_00135; trypsin-like peptidase	0.024	1.408	1.849	2.536	2.983	3.508
CCNA_00247; two-component receiver protein SpdR	-0.022	0.746	1.113	2.001	1.936	2.122
CCNA_00527; conserved hypothetical protein	0.015	0.266	0.896	2.136	3.469	4.796
CCNA_00543; methyl-accepting chemotaxis protein	0.009	1.134	1.716	2.128	2.157	2.226
CCNA_00551; hypothetical protein	-0.004	0.866	1.543	2.139	2.308	2.69
CCNA_00554; methyltransferase	-0.001	0.062	0.822	2.006	2.545	2.978
CCNA_00908; 3-oxoacyl-(acyl-carrier-protein) synthase III	0	0.407	0.586	0.845	1.489	2.322
CCNA_00948; CtrA inhibitory protein SciP	0.007	1.162	1.949	2.067	2.008	2.039
CCNA_01020; LacI-family transcriptional regulator	0.007	0.551	1.386	2.301	2.185	2.402
CCNA_01214; YjgP/YjgQ family membrane permease	0.015	2.881	3.481	3.156	3.126	3.309
CCNA_01215; histidine triad (HIT) hydrolase	0.028	1.556	1.748	1.705	2.032	2.724
CCNA_01345; short chain dehydrogenase	0.005	0.092	0.3	0.598	1.441	2.418
CCNA_01354; myo-inositol 2-dehydrogenase IdhA	0.011	0.138	0.551	0.717	1.425	2.056
CCNA_01893; SnoaL-like domain protein	-0.014	0.189	0.498	0.484	1.23	2.187
CCNA_02087; deoxyguanosinetriphosphate	0.002	0.592	1.448	1.871	2.344	2.614

triphosphohydrolase						
CCNA_02125; polar development protein podJ	0.008	1.149	2.18	2.796	3.456	4.419
CCNA_02242; PHB granule-associated protein, phasin2	-0.018	0.695	1.362	1.519	1.819	2.214
CCNA_02415; Xre-family transcriptional regulator	0.001	-0.156	2.237	3.038	2.641	2.593
CCNA_02619; stomatin/prohibitin-related protein	-0.013	0.45	1.896	3.271	3.38	3.866
CCNA_02722; conserved hypothetical protein	0.002	0.867	1.936	2.676	3.336	4.092
CCNA_02846; DegP/HtrA-family serine protease	0.018	0.267	1.041	1.554	1.965	2.587
CCNA_02880; terminase-like family protein	-0.003	0.224	0.389	0.732	1.32	2.122
CCNA_02934; conserved hypothetical protein	-0.003	0.633	1.144	2.146	2.127	2.572
CCNA_03099; hypothetical protein	0.002	0.378	0.678	1.271	1.525	2.473
CCNA_03161; transcriptional regulator xylR	0.017	1.201	1.769	2.792	2.9	2.983
CCNA_03386; multimodular transpeptidase-transglycosylase PbpC	0.002	0.775	1.546	2.13	2.477	2.602
CCNA_03465; glycine cleavage system aminomethyltransferase T	0.012	1.186	1.447	1.937	2.076	2.344
CCNA_03611; glutathione-regulated potassium-efflux system protein kefC	0.005	-0.076	1.577	2.82	3.551	3.907
CCNA_03803; acetyltransferase family holdfast biogenesis protein HfsK	-0.003	0.895	1.957	2.71	3.132	3.698
CCNA_03902; conserved hypothetical protein	-0.009	0.681	1.566	2.037	2.339	3.165

Table S3 *Fitness scores across cheesecloth passages for mutant clusters shown in Fig 1C*
Fitness values represent the average of the three replicates for each passage. The first passage without cheesecloth (PYE1) represents the time 0 sample.

Genotype	Deletion (PYE)	Empty vector (PYE)	Complement (PYE)	Deletion (M2X)	Empty Vector (M2X)	Complement (M2X)
Wild-type	1.00 ± 0.03	n.m.	n.m.	1.00 ± 0.06	n.m.	n.m.
Δ*hfiA*	1.28 ± 0.16	n.m.	n.m.	4.34 ± 0.23	n.m.	n.m.
Δ*hfsJ*	0.00 ± 0.00	n.m.	n.m.	0.00 ± 0.00	n.m.	n.m.
Δ*CCNA_01242*	0.68 ± 0.06	0.98 ± 0.06	0.98 ± 0.13	0.81 ± 0.19	0.74 ± 0.09	1.09 ± 0.17
Δ*hfaE*	0.34 ± 0.08	0.32 ± 0.12	1.02 ± 0.08	0.06 ± 0.03	0.05 ± 0.02	1.08 ± 0.19
Δ*hfsL*	0.00 ± 0.00	0.00 ± 0.00	1.00 ± 0.12	0.00 ± 0.01	0.00 ± 0.01	1.10 ± 0.21
Δ*CCNA_00497*	1.12 ± 0.07	1.02 ± 0.07	1.08 ± 0.04	2.10 ± 0.23	3.47 ± 0.35	0.84 ± 0.10
Δ*CCNA_02386*	0.72 ± 0.07	0.68 ± 0.08	1.10 ± 0.14	1.97 ± 0.30	2.73 ± 0.19	0.72 ± 0.13
Δ*rfbB*	1.34 ± 0.06	1.40 ± 0.03	1.08 ± 0.07	3.24 ± 0.71	2.14 ± 0.24	1.48 ± 0.31
Δ*wbqP*	1.29 ± 0.11	1.09 ± 0.11	1.11 ± 0.12	3.87 ± 0.51	2.31 ± 0.40	1.10 ± 0.26
Δ*flgH*	0.58 ± 0.05	0.62 ± 0.06	1.03 ± 0.04	2.91 ± 0.08	2.42 ± 0.26	1.23 ± 0.25
Δ*cpaH*	0.71 ± 0.05	0.76 ± 0.08	1.03 ± 0.07	2.68 ± 0.07	1.85 ± 0.24	0.90 ± 0.31
Δ*pilA*	0.34 ± 0.04	0.44 ± 0.04	1.01 ± 0.06	0.20 ± 0.16	0.08 ± 0.05	0.93 ± 0.36

875
876 **Table S4** *Complementation of adhesion defects*
877 Normalized crystal violet staining values are shown as the average ± standard deviation from at
878 least 4 biological replicates. All values shown reflect trends that were consistent across at least
879 five independent experiments. Cells were grown for 17 hours in M2X or 24 hours in PYE medium
880 before staining. n.m. – not measured.
881

Genotype	Deletion (PYE)	ΔhfiA (PYE)	ΔpleD (PYE)	Deletion (M2X)	ΔhfiA (M2X)	ΔpleD (M2X)
Wild-type	1.00 ± 0.03	1.28 ± 0.16	0.81 ± 0.01	1.00 ± 0.06	5.61 ± 0.27	1.38 ± 0.19
Δ*hfiA*	1.28 ± 0.16	n.m.	1.08 ± 0.07	4.34 ± 0.23	n.m.	5.53 ± 0.16
Δ*hfsJ*	0.00 ± 0.00	n.m.	n.m.	0.00 ± 0.00	n.m.	n.m.
Δ*wbqP* Δ*hfsJ*	0.48 ± 0.25	n.m.	n.m.	2.51 ± 0.64	n.m.	n.m.
Δ*flgH*	0.58 ± 0.05	0.62 ± 0.07	0.31 ± 0.02	2.91 ± 0.08	2.78 ± 0.21	1.41 ± 0.33
Δ*cpaH*	0.71 ± 0.05	0.91 ± 0.05	0.19 ± 0.01	2.68 ± 0.07	4.29 ± 0.16	1.22 ± 0.18
Δ*pilA*	0.34 ± 0.04	0.73 ± 0.03	0.43 ± 0.01	0.20 ± 0.16	5.95 ± 0.18	0.25 ± 0.08
Δ*flgH* Δ*hfsJ*	0.00 ± 0.00	n.m.	n.m.	0.01 ± 0.01	n.m.	n.m.
Δ*cpaH* Δ*hfsJ*	0.00 ± 0.00	n.m.	n.m.	0.01 ± 0.02	n.m.	n.m.
Δ*flgH* Δ*cpaH*	0.40 ± 0.01	n.m.	n.m.	4.13 ± 0.18	n.m.	n.m.
Δ*flgH* Δ*pilA*	0.32 ± 0.02	n.m.	n.m.	2.00 ± 0.25	n.m.	n.m.
Δ*cpaH* Δ*pilA*	0.43 ± 0.03	n.m.	n.m.	0.12 ± 0.04	n.m.	n.m.

Table S5 *Additional adhesion phenotypes for motility mutants*
Normalized crystal violet staining values are shown as the average ± standard deviation from at least 4 biological replicates. All values shown reflect trends that were consistent across at least five independent experiments. Cells were grown for 17 hours in M2X or 24 hours in PYE medium before staining. n.m. – not measured.

Strain	PYE	M2X
Wild-type	0.686 ± 0.045 (739)	0.081 ± 0.006 (743)
Δ*hfiA*	0.863 ± 0.021 (526)	0.722 ± 0.039 (703)
Δ*hfsJ*	0.000 ± 0.000 (628)	0.000 ± 0.000 (638)
Δ*flgH*	0.869 ± 0.037 (662)	0.620 ± 0.013 (609)
Δ*cpaH*	0.874 ± 0.031 (531)	0.296 ± 0.094 (689)
Δ*pilA*	0.673 ± 0.030 (464)	0.092 ± 0.016 (367)
Δ*pleD*	0.496 ± 0.024 (457)	0.084 ± 0.007 (500)

Table S6 *Holdfast counts for motility mutants*
The values represent the fraction of cells (out of 1) that stained with a holdfast focus with the associated standard deviation from three biological replicates. The total number of cells counted is shown in parentheses. Cells were harvested from low-density cultures (Material and Methods) to minimize the formation of rosettes. However, in the event that rosettes were observed, all cells in the rosette were counted as holdfast producing.

897

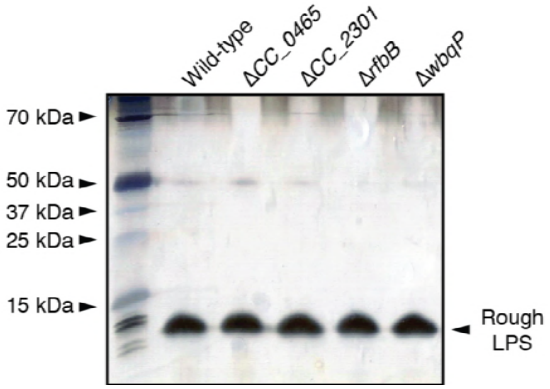

898
899
900 **Figure S1** *Analysis of rough LPS in SLPS mutants* Rough LPS was isolated and analyzed as
901 described in materials and methods. None of the four SLPS mutants show apparent defects in
902 rough LPS.
903

904

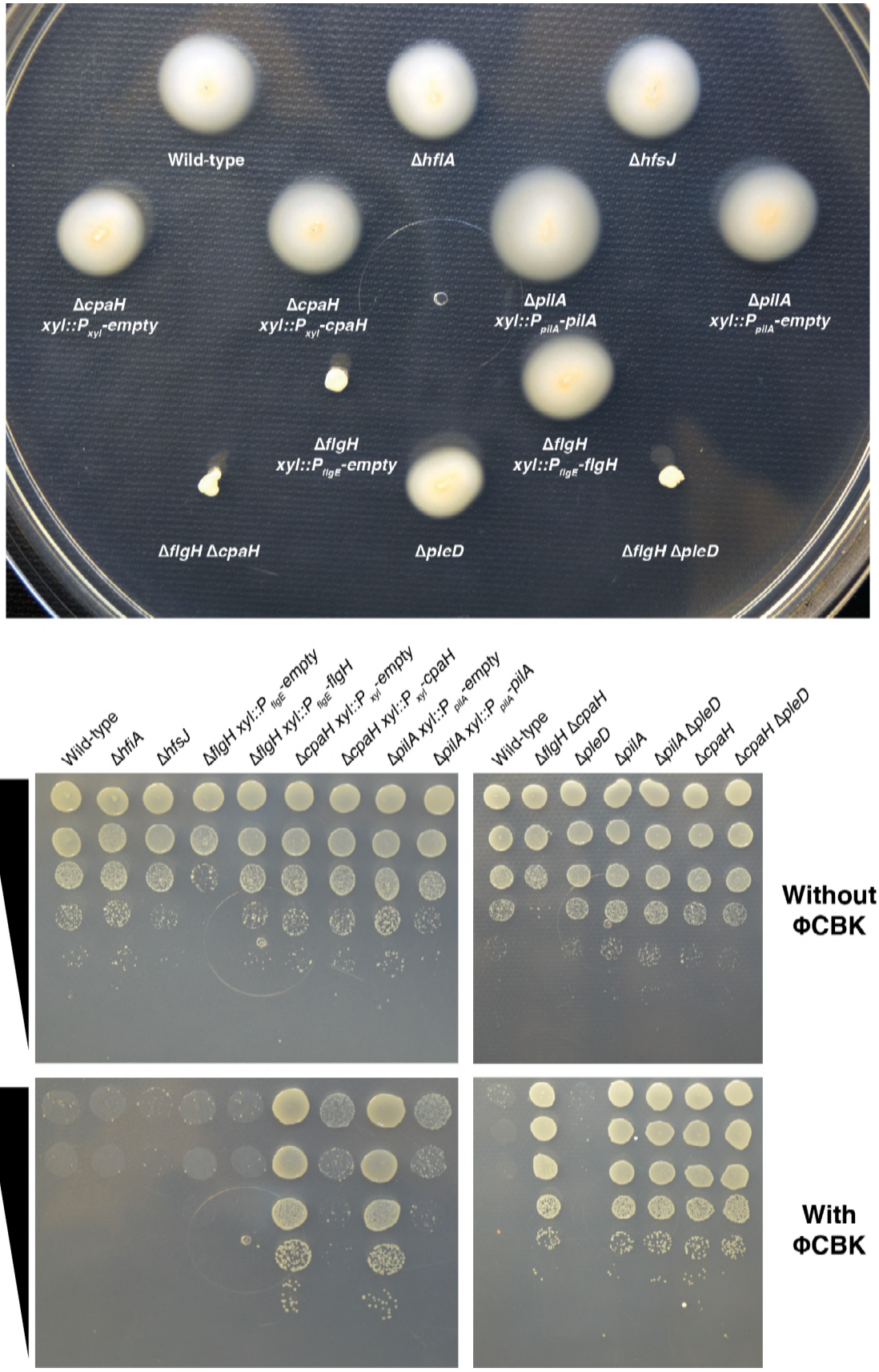

905
906 **Figure S2** *Validation of pilus and flagellum phenotypes in polar appendage mutants*

907 Top: Swimming phenotypes for relevant mutants are shown. Note that Δ*pilA* has a slight but
908 reproducible increase in swarm size that can be complemented by ectopic expression of *pilA* in
909 trans. Mutants lacking *flgH* show the expected non-motile phenotype. Bottom: ΦCBK sensitivity of
910 motility mutants. Mutants lacking *pilA* or *cpaH* show the expected ΦCBK resistance phenotype.
911

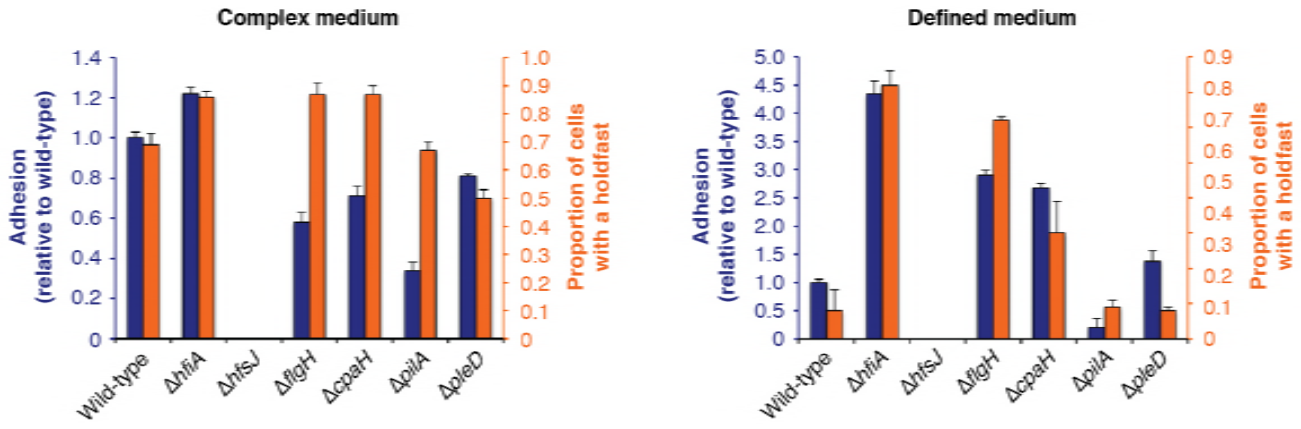

912
913 **Figure S3** *Comparison of crystal violet staining and holdfast counts for motility mutants*
914 Surface attachment was assessed by CV staining (violet bars) and holdfast production by fWGA
915 staining (orange bars) as described in Material and Methods. The values for growth in complex
916 medium are shown on the left and defined medium on the right.
917
918

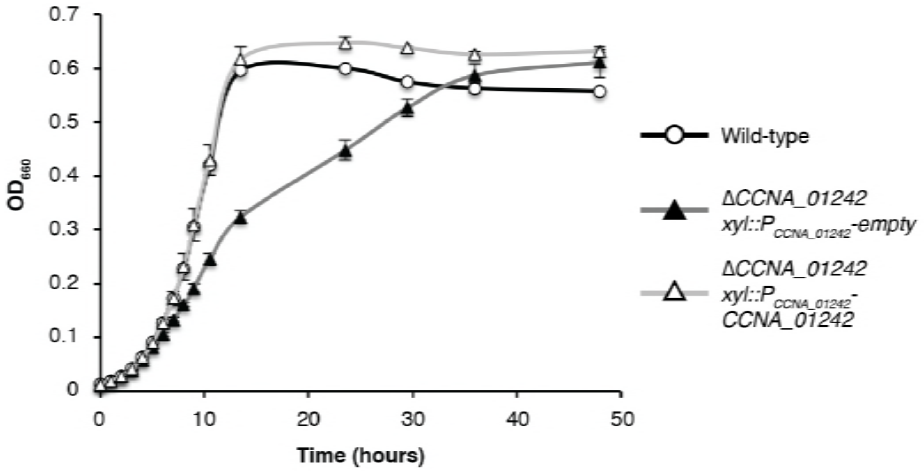

Figure S4 *Complementation of growth defect in Δ*CCNA_01242
The Δ*CCNA_01242* mutant displays a biphasic growth curve indicating a defect. Normal growth is restored by ectopic complementation with *CCNA_01242.*